Variation in bacterial composition, diversity, and activity across different subglacial basal ice types

Shawn M. Doyle[a] and Brent C. Christner[b]

[a]Department of Oceanography, Texas A&M University, College Station, TX, USA.
[b]Department of Microbiology and Cell Science, University of Florida, Gainesville, FL, USA.

Running title: **Bacterial community structures in basal ice types**

Abstract word count: 250
Importance word count: 140
Article word count: 5485

*Corresponding author:
Shawn M. Doyle
Department of Oceanography
Texas A&M University
Eller O&M Bldg, Rm 716D
College Station, TX, 77843-3146
Tel: 979-845-5105
E-mail: shawndoyle@tamu.edu

Competing Interests: The authors declare no competing financial interests.

ABSTRACT

Glaciers and ice sheets possess layers of basal ice characterized by high amounts of entrained debris that can serve as sources of nutrients and organic matter, providing habitat for microorganisms adapted to the frozen conditions. Basal ice forms through various mechanisms and is classified based on its ice and debris content; however, little is known about variation in microbial composition, diversity, and activity across different basal ice types. We investigated these parameters in four different types of basal ice from a cold-based and temperate glacier and used a meta-analysis to compare our findings with microbiome studies from other frozen environments. We found basal ice environments harbor a diverse range of microbiomes whose composition and activity can vary significantly between basal ice types, even within adjacent facies from the same glacier. In some debris-rich basal ices, elevated ATP concentrations, isotopic gas signatures, and high ratios of amplified sequences for 16S rRNA relative to that for 16S rRNA genes implicated certain bacterial taxa (e.g., *Paenisporosarcina*, *Desulfocapsa*, *Syntrophus, Desulfosporosinus*) as being potentially active, with ice temperature appearing to be an important predictor for the diversity of taxa inferred to be active. Compared to those of other sympagic environments, these microbiomes often resembled those found in permafrost or perennial cave ice rather than other glacial ice environments. In contrast, debris-poor basal ices harbored microbiomes more like those found in oligotrophic englacial ice. Collectively, these results suggest that different basal ice types contain distinct microbiomes that are actively structured by the diagenesis of their habitat.

IMPORTANCE

The discharge of material from the basal ice zones of glaciers and ice sheets is an important source of dissolved organic matter, nutrients, and trace metals to downstream environments. Microorganisms with the ability to remain metabolically active while frozen have the potential to alter these substrates before they are released and may thus be a vital biogeochemical component of proglacial environments. However, basal ice environments are among the least explored areas of the cryosphere and information on their microbiology is limited. Here, we examine several basal ice types that were collected from different glaciers to investigate how their microbiomes varied. Our results indicate that sediment-rich basal ice from cold-based and temperate glaciers harbor microbiomes that conduct biogeochemical transformations at subzero temperatures and raises the intriguing possibility that subsurface regions of the cryosphere may be more biogeochemically active than previously thought.

1. INTRODUCTION

At the ice-bed interface of a glacier or ice sheet, basal ice forms when subglacial debris and/or water is incorporated into the base of the ice mass through mechanisms such as freeze-on, regelation, or incorporation of pre-existing ice (1, 2) . Basal ice has a physical structure, chemistry, and microbial composition that is directly affected by its proximity to and interaction with material beneath the glacier (1, 3, 4). When frictional or geothermal heating create temperate conditions at the bed, the melting of basal ice can provide inputs of organic matter, nutrients, oxidants, and microorganisms to the subglacial environment (5). Hence, basal ice likely represents an important vector for dispersing microbes in subglacial aquatic environments that exist within the glacier's flow path (6).

Basal ice layers contain debris entrained from the underlying substrate that ranges in size from fine-grained clays and silts to coarse sands, gravels, and boulders. Basal ice formation can produce layering and stratification patterns that become deformed by the folding and shearing forces associated with glacier flow (7). These processes of entraining and restructuring of subglacial debris combine to produce distinct types of basal ice. This ranges from relatively debris-poor types containing <1% (w/v) sediment to debris-rich types composed almost entirely of sediment with only interstitial ice (1). When compared to the overlying englacial ice (i.e., derived from snowfall), the sediment-rich basal ice contains higher concentrations of potential microbial substrates that include formate, acetate, ferrous iron, and ammonia (8–11). These compounds are hypothesized to be an important source of electron donors for heterotrophic and lithotrophic microorganisms inhabiting subglacial environments, including frozen matrices within the basal ice itself (4, 12).

Although ecosystems associated with sympagic environments were first described nearly 60 years ago (13), viable microorganisms entrapped within glacial ice have been assumed to exist in a persistent state of metabolic dormancy (14). This view has been challenged based on evidence from several pioneering studies that revealed anomalies in entrapped gas concentrations within englacial (15, 16) and basal ice (17–19). The metabolic activity of microorganisms in basal ice is now thought to play an important role in the biogeochemistry of downstream terrestrial, freshwater, and marine environments that receive seasonal discharges of basal ice and subglacial meltwater (20–23). In fact, transport of basal material is one of the largest sources of labile dissolved organic carbon and iron to marine systems receiving outflow from glaciated watersheds (24–26).

The world's ice sheets are estimated to contain ~10.2 Pg of organic carbon (27), which represents only ~0.5% of the global soil organic carbon pool (28). However, the sediments underlying the Greenland and Antarctic ice sheets may contain reservoirs of ~500 and ~21,000 Pg of organic carbon, respectively (29, 30). Due to accelerated rates of melt and glacial retreat in the polar regions, the products of organic matter processing by subglacial microorganisms may play an increasingly important role in global carbon cycling. For example, the subglacial production of biogenic methane and its subsequent release to the atmosphere could represent a positive feedback that accelerates further climate warming (30). Indeed, basal ice sediments have been shown to contain viable methanogens (8, 31) as well as methanotrophs (32, 33), indicating the presence of a subglacial methane cycling. Microbial activities in the basal zones of the world's glaciers and ice sheets may thus be an overlooked component of Earth's climate oscillations over geologic timeframes. Despite their potential importance, the logistic challenges associated

130 with accessing these environments have contributed to the dearth of information on the
131 microbes and biogeochemical processes they perform in the basal zone of large ice masses.
132 In this study, we used 16S rRNA gene amplicon sequencing to profile the
133 composition and structure of microbial assemblages within basal ice types and from
134 different locations. To explore how these microbial assemblages compare to those in other
135 perennially frozen environments, we performed a meta-analysis that combined our data
136 with that from other studies. Many of these studies sequenced different variable regions of
137 the 16S rRNA gene (e.g., V4, V2, V3V4) that do not fully overlap, hindering the use of
138 traditional OTU-based approaches. To address this, we used the SATé-enabled phylogenetic
139 placement (SEPP) technique to insert exact amplicon sequence variants (ASVs) from these
140 heterogenous variable regions into the same reference phylogeny (34). This enables a
141 phylogenetically stable comparison of the microbial assemblages inhabiting these different
142 frozen environments. In contrast to the aeolian-source microbes in englacial ice, the
143 microorganisms in basal ice appear to represent "communities" in an ecological sense. We
144 also used RNA- and ATP-based approaches to identify potentially active taxa and regions in
145 basal ice types and discuss the implications of microbial processes that occur in an
146 important transient environment of the cryosphere.
147

148 **2. MATERIALS AND METHODS**

149 **2.1 Ice sampling**

150 *Taylor Glacier*

151 Taylor Glacier is a cold-based glacier (i.e., has basal ice that is constantly below the
152 pressure-melting point) that is an outlet of the East Antarctic Ice Sheet, terminating at the

western end of Taylor Valley (McMurdo Dry Valleys, Victoria Land, Antarctica). During the austral summers of 2007 and 2009, two tunnels were excavated into the basal zone of the northern lateral margin of the glacier (Fig. S1). Tunnel construction was initiated on fresh ice aprons and extended ~8 m into the glacier interior. At the end of each tunnel, a vertical shaft (2007 expedition) or large chamber (2009 expedition) was excavated to expose a stratigraphic sequence of multiple basal ice types (4). Electric chainsaws equipped with unlubricated carbide tipped chains were used to exhume samples of the ice sequence from each basal ice type. Ice samples were sealed in polypropylene flat wrap, packed into insulated containers, and shipped frozen from the field to Louisiana State University where they were subsequently stored at -20 °C.

Matanuska Glacier

Matanuska Glacier is a 43 km temperate (i.e., englacial and basal ice constantly at the pressure melting point), valley glacier located in south-central Alaska, approximately 140 km northeast of Anchorage. In July 2013, a horizon of debris-rich basal ice exposed near the glacier terminus was sampled using an electric chainsaw (Fig. S2). After collection, the ice samples were packaged in polypropylene flat wrap and shipped frozen to Louisiana State University for storage at -20 °C.

2.2 Ice decontamination

Within a temperature-controlled environmental room (-5°C), ~2 kg of ice was cut from larger basal ice samples using either a band saw (for the sediment-poor basal ice) or a diamond-bladed masonry saw (sediment-rich basal ice). The surface of freshly cut samples were then cleaned following previous methods (35). Briefly, the outermost surface was physically removed by scraping with an autoclaved microtome blade and the newly

176 exposed ice surface was then washed with chilled (-5°C), 0.22 μm filtered 95% ethanol.
177 Microtome scraping was omitted when processing sediment-rich samples due to the
178 presence of coarse granules and stones embedded in the sediment-layers. Following the
179 ethanol wash, samples were washed extensively with ice-cold, 0.22 μm, twice-autoclaved
180 deionized water until a minimum of ~5 mm of the outer surface had been removed based
181 on the ice weight. Large, sterilized surgical forceps were used to handle all ice samples
182 during decontamination and were exchanged frequently during the procedure to prevent
183 carryover contamination. Sample weights before and after decontamination were used to
184 estimate the amount of material removed from each sample during processing, which was
185 typically between 15% and 25% of the initial mass.

186 The effectiveness of the decontamination procedure was monitored by coating ice
187 samples beforehand with a tracer solution that consisted of three components: [1] ~10^8
188 cells mL^{-1} of *E. coli* JM109 cells transformed with a pETBlue-2 plasmid (Novagen)
189 containing the gene for alcohol dehydrogenase (ADH) from *Drosophila melanogaster*, [2]
190 fluorescein (1000 ppm), and [3] 33% (v/v) glycerol to prevent freezing on the ice at -5°C.
191 The removal of the tracer was monitored after each step of the decontamination procedure
192 (i.e., scraping, ethanol wash, H_2O wash). The fluorescein fluorophore component was
193 monitored by quantifying blue-green fluorescence in 200 μL of rinse-water or meltwater
194 using a BioTurner 20/20n Luminometer (P/N 2030-002) equipped with the blue
195 fluorescence module (BioTurner 2030-041). The pETBlue-2 plasmid component was
196 monitored using a PCR with the following conditions: 1 U of Taq DNA polymerase
197 (5PRIME), 1× MasterTaq buffer, 1× TaqMaster PCR enhancer, 1.5 mM Mg^{2+}, 0.2 μM of each
198 primer (TF7: 5'-TAATACGACTCACTATAGGG -3'; pETBlue-DOWN: 5'-

199 GTTAAATTGCTAACGCAGTCA-3'), 200 μM dNTPs, and ~100 pg of template DNA. Thirty
200 cycles of PCR were done with a 30 s denaturation step at 94 °C, 60 s annealing step at 55 °C
201 and extension at 72 °C for 60 s, followed by a final extension at 72 °C for 10 min. The
202 presence of viable *E. coli* was monitored by spread plating rinse-water and meltwater on
203 agar-solidified LB media containing ampicillin (100 μg mL^{-1}) followed by overnight
204 incubation at 37 °C. Samples in which any component of the tracer solution was detected in
205 the final meltwater were discarded and reprocessed from a new subsample.

206 **2.3 ATP analysis**

207 Immediately after melting, samples were filtered through 0.22 μm pore size
208 polyethersulfone (Supor; Pall) filters using a bench-top vacuum manifold (≤ 20 kPa). Clean
209 ice samples were filtered through a 25 mm diameter filter while banded, solid, and
210 dispersed ice samples were processed through either a 47 mm or 90 mm diameter filter,
211 depending on total sediment content. The filters were cut into small pieces using a sterile
212 scalpel and extracted by vortexing for 10 s in 5 mL of boiling Tris-acetate buffer (TAB;
213 50mM Tris base adjusted to pH 7.75 with acetic acid). The mixture was then incubated in a
214 boiling water bath for 5 minutes and immediately placed on ice for 30 minutes. Following
215 centrifugation for 5 minutes at 4500×g to remove debris, the supernatant was collected.

216 The concentration of extracted ATP was measured using a modification of the firefly
217 luciferase-luciferin assay described by (36). Briefly, 10 μL of extract was added to an equal
218 volume of triethanolamine buffer (TEOA buffer; 200 mM triethanolamine pH 7.6, 2 mM
219 MgCl2, 240 mM KCL) and incubated at 37°C for 10 minutes. To correct for adenylate
220 adsorption to and luciferase inhibition by the sediment in the sample extracts, two samples
221 were prepared in parallel for each measurement. Following incubation at 37°C, 10 uL of

222 TAB supplemented with 10 μM ATP was added to one of the samples, providing an internal
223 standard for each measurement. All samples were kept on ice during preparation and were
224 equilibrated to room temperature (22 °C) prior to the addition of luciferase and
225 measurement of luminescence.

226 Weighted linear regression was used to generate calibration curves using
227 concentrations of ATP (in TAB) from 1 pM to 10 μM. The luciferase-luciferin cocktail was
228 prepared fresh for each series of measurements and consisted of 100 U ml^{-1} luciferase and
229 0.140 mM D-luciferin. Luminescence was quantified with a 20/20n luminometer
230 (Promega) using auto-injection of 100 μL of the luciferase-luciferin cocktail. Relative
231 luminescence units (RLU) were integrated for three seconds immediately after injection.
232 Sample RLU values were corrected for adsorption and inhibition using the following
233 formula:

$$\frac{1}{\left(\frac{RLU_{\text{sample+std}} - RLU_{\text{sample}}}{RLU_{\text{blank+std}}}\right)} \times RLU_{\text{sample}} = RLU_{\text{corrected}}$$

234 The corrected RLU values were used together with the standard calibration curve to
235 determine the ATP concentration in the extractant. Final ATP concentrations were
236 corrected for dilution and divided by the mass of the ice sampled. All values reported are
237 the means of replicate samples (n = 3 to 5).

238 **2.4 Nucleic acid extraction**

239 Decontaminated basal ice samples were placed in sterilized containers and melted
240 at 4°C. For samples from sediment-rich basal ice (i.e., banded, solid, and dispersed ice), the
241 resulting meltwater was shaken to resuspend any sediment and DNA was extracted from
242 the resulting meltwater-sediment slurry using MoBio PowerMax DNA Isolation kits. To

243 increase DNA extraction yields, two 10g extractions were combined onto a single silica spin
244 column for each sample. For samples from sediment-poor basal ice (i.e., clean ice),
245 meltwater was filtered onto 47 mm, 0.22 μm pore size Supor PES filter membranes (Pall)
246 with ≤20 cm Hg of vacuum. DNA was extracted from the filters using MoBio PowerWater
247 DNA Isolation kits as per the manufacturer's instructions with one exception: the
248 mechanical lysis step was performed on a BioSpec MiniBeadbeater-8 for 2 minutes at
249 maximum speed. All DNA samples were stored at -80°C until PCR amplification.
250 Due to the low cell abundances in the basal ice (≤10^4 cells g^{-1}; (3)), very large
251 samples (~5 kg of ice; Table S1A) were processed to recover sufficient RNA for reverse
252 transcription PCR (RT-PCR). To facilitate filtration of the large sample sizes, coarse
253 sediment was removed from sediment-rich basal ice samples after melting using low speed
254 centrifugation (700×g, 10 min, 4°C). The resulting supernatant containing fine clay and silt-
255 like particles was then concentrated onto 90 mm, 0.22 μm pore size Supor PES filter
256 membranes. Meltwater from clean ice samples did not require this centrifugation step and
257 were directly filtered onto 90mm, 0.22 μm pore size Supor PES filters.
258 After filtration, the filters were immediately processed for RNA extraction using a
259 modified phenol-chloroform extraction protocol (32). Briefly, filters were sliced into small
260 pieces using a sterile scalpel, immersed in 3 mL of TE buffer (1 mM EDTA, 10 mM Tris; pH
261 6.3) containing lysozyme (15 mg mL^{-1}), and vortexed for 30 minutes at room temperature.
262 Samples were then homogenized in a BioSpec Mini-Beadbeater for 2 minutes at maximum
263 speed using ~1 g of sterilized 0.1 mm diameter zirconia/silica beads. After bead beating,
264 crude extracts were amended with two volumes of chilled (4°C) denaturing buffer (4M
265 guanidine thiocyanate, 50 mM Tris, 10 mM EDTA, 1% w/v N-lauroylsarcosine, 1% β-

266 mercaptoethanol), the resulting insoluble material was pelleted via centrifugation (4500×g
267 for 5 min at 4°C), and the supernatant was collected. The pellet was washed with 3 mL of
268 chilled denaturing buffer, centrifuged again, and the resulting supernatant pooled with the
269 first. This pooled lysate was then extracted with an equal volume of
270 phenol:chloroform:isoamyl alcohol (25:24:1, pH 6.6), followed by a second extraction with
271 chloroform:isoamyl alcohol (24:1). Nucleic acids were purified from these extracts via an
272 overnight ethanol precipitation with 0.3 M sodium acetate (pH 6.0). Linear acrylamide (20
273 μg mL^{-1}; Ambion) was used as a coprecipitant to aid recovery. Genomic DNA was
274 eliminated from RNA extracts by digesting for one hour at 37°C with 4 U of TURBO DNAase
275 (Ambion) followed by purification with MEGAclear Transcription Clean-Up kits (Ambion).
276 Extracted DNA and RNA concentrations were measured using Quant-it Picogreen
277 and Ribogreen kits (Life Technologies), respectively, per the manufacturer's instructions.

278 **2.5 16S rRNA amplicon sequencing**

279 From the extracted RNA, complementary DNA (cDNA) was reverse transcribed from
280 ~1 ng of total RNA using SuperScript II reverse transcriptase with the 806R primer (5'-
281 GGACTACVSGGGTATCTAAT-3') following the manufacturer's protocol. Controls lacking
282 RNA template or reverse transcriptase were analyzed to monitor for contaminating RNA
283 and the persistence of genomic DNA, respectively, in the samples.
284 The hyper-variable V4 region of the 16S rRNA gene was PCR amplified from the
285 DNA extracts and cDNA libraries using a barcoded 515F-806R primer pair (37). Each 50 μL
286 PCR contained ~100 pg of DNA or cDNA, 2.5 U of AmpliTaq Gold DNA polymerase LD
287 (Invitrogen), 1× Gold Buffer, 2.5 mM $MgCl_2$, 0.2 μM of each primer, and 0.2 μM dNTPs.
288 Amplification conditions included at 95°C for 9 min, followed by 30 to 40 cycles of

289 denaturation at 94°C for 1 min, annealing at 50°C for 30 s, and extension at 72°C for 30 s. A
290 final extension was performed at 72°C for 10 min.

291 Following amplification, amplicons were separated by electrophoresis on a 2%
292 agarose gel to assess relative band intensity and size. The amplicons were quantified with
293 Quant-it fluorometry and pooled at equimolar concentrations. Two extraction blanks were
294 included in the pooled libraries to serve as procedural controls (38, 39). Pooled libraries
295 were purified with a MoBio UltraClean PCR Cleanup Kit and sequenced on the Illumina
296 MiSeq platform (v2 chemistry, 2× 250 bp; Georgia Genomics Facility).

297 **2.6 16S rRNA amplicon analysis**

298 Sequence read curation and processing was performed using DADA2 (40) with the
299 following filtering parameters (maxN=0, trunQ=2, rm.phix=TRUE, maxEE=2, R1
300 truncLen=240, R2 truncLen=200). Error rates for the filtered and trimmed R1 and R2 reads
301 were calculated using the *learnErrors* function and subsequently used to denoise reads
302 using the DADA2 sample inference algorithm. The denoised reads were merged into
303 amplicon sequence variants (ASV) using a global ends-free alignment. Paired reads
304 containing mismatches in the overlapping region were removed from the dataset. Chimeric
305 ASVs were identified and removed by using the consensus method within the
306 *removeBimeraDenovo* function. A consensus taxonomy for each ASV was then assigned
307 using a naïve Bayesian classifier (41) trained on release 132 of the SILVA reference
308 database (42). The dataset was then subsampled to an even read depth across all samples
309 (59,562 sequences). Any ASV classified as a chloroplast, mitochondria, or from which
310 ≥0.1% of its reads were from a procedural blank were removed. ASVs observed exclusively

311 in the RNA libraries were flagged as a potential contaminant and removed from the
312 analysis.

313 **2.7 Meta-analyses of microbiomes of perennially frozen ecosystems**

314 Publicly available datasets on the NCBI Sequence Read Archive (SRA) from
315 perennially freshwater frozen environments were identified using a search on August 8th,
316 2021 with the following syntax: ice metagenome[Organism], glacier
317 metagenome[Organism], and permafrost metagenome[Organism]. Run tables from
318 unambiguously labeled 16S rRNA amplicon datasets were aggregated and studies based on
319 Sanger sequencing were excluded; only datasets based on Illumina, 454, or IonTorrent
320 sequencing were considered in the analysis. Because many studies contained samples from
321 laboratory experiments or field manipulations (e.g., nutrient amendment, thawing, etc.),
322 each dataset was manually curated and cross-referenced with a publication or other data
323 source so that only high quality 16S rRNA surveys from genuine, unmodified permanently
324 frozen environments were included. As part of this effort, datasets were filtered to remove
325 samples from environments that were only seasonally frozen. For example, samples of an
326 active soil layer or transition zone from permafrost datasets were excluded. Additionally,
327 because of their marine origin, we also choose to exclude the wealth of sea ice sample data
328 available and focus the analysis on terrestrial icy environments. Unfortunately, several
329 datasets also had to be excluded because their sequence reads on the SRA were not
330 demultiplexed and barcode information was not provided in the linked metadata or
331 publication. A list of datasets that met these criteria and were included in the meta-analysis
332 are detailed in Table S1B. All runs were downloaded using the SRA Toolbox *fastq-dump*
333 function.

334 Each dataset was individually processed using DADA2 to infer ASV sequences and
335 produce an ASV table. For each study, the filtering parameters were adjusted to account for
336 variation in fragment length and the 16S rRNA variable region sequenced. Due to higher
337 rates of homopolymer and indel errors with 454 and IonTorrent sequencing, datasets using
338 these platforms used a band size parameter of 32 and homopolymer region (≥ 3 repeated
339 bases) gap cost of -1 during the sample inference algorithm. For Illumina datasets, the band
340 size parameter was set to 16 and gaps in homopolymer regions were treated as normal
341 gaps (gap cost of -8). Nine datasets had to be removed from the meta-analysis after these
342 steps due to the loss of too many sequences during quality control steps within the DADA2
343 pipeline. Complete parameter details and throughput statistics for each dataset in the final
344 meta-analysis are available in Table S1C and S1D. In datasets containing clearly labeled
345 replicates, read counts from replicate samples were combined and averaged before
346 downstream analyses.

347 ASV sequences from each study were merged and inserted into the 99% Greengenes
348 reference tree (43) using the SATé-enabled phylogenetic placement (SEPP) technique (44)
349 within the QIIME2 *fragment-insertion* plugin (34). The merged ASV tables from each study
350 were filtered to remove ASVs rejected from tree insertion by SEPP. ASVs which could not
351 be taxonomically classified beyond the domain rank (n=2434) or were classified as
352 mitochondrial sequences (n=119) were flagged as potential artifacts and removed.

353 The statistical significance of hierarchical clustering patterns between samples in
354 the meta-analysis was performed using Monte Carlo simulations of pairwise unifrac
355 distances as implemented in the *sigclust2* R package (45). Because parallelized, matrix-
356 based unifrac calculators are incompatible with *sigclust2*, we used the serial, pairwise

357 unifrac calculator from the *scikit-bio* python package. This calculator was embedded into R
358 for the *sigclust2* Monte Carlo simulations using the *reticulate* R package.

359 **2.8 Data availability**

360 Sequence read data generated in this study is available on NCBI SRA under
361 BioProject PRJNA282540.

362

363 **3. RESULTS**

364 **3.1 Description of Basal Ice Samples**

365 Based on the nomenclature of (46), we identified three distinct types of basal ice in
366 the basal ice profiles sampled from Taylor Glacier: clean ice, banded ice, and solid ice
367 (Table 1; Fig. S3; (4)). All three types were collected during the 2007 expedition, while only
368 clean ice and banded ice horizons were targeted during the 2009 expedition. The basal ice
369 recovered from Matanuska Glacier was identified as dispersed ice and was the only type
370 observed at the location of sampling.

371 **3.2 Biomass in sediment-rich and sediment-poor basal ice**

372 The quantity of DNA and RNA extracted from the basal ices was divided by the
373 sample mass to assess the relative amounts of microbial biomass present within each basal
374 ice type. Approximately 10,000-fold more DNA per gram of basal ice was extractable from
375 the sediment-rich basal ice types (i.e., banded, solid, and dispersed) than in the sediment-
376 poor clean ice (Table 2). Assuming a bacterial genome weight of 2.5 fg, the concentration of
377 DNA extracted from the clean Taylor Glacier basal ice corresponds to 560 genomes per
378 gram of ice, which agrees well with direct cell counts of samples from this ice facies (Table
379 2; (3, 4)). In contrast, genome abundances inferred from DNA concentrations in the

380 sediment-rich Taylor Glacier basal ice samples were two to three orders of magnitude
381 higher than direct cells counts. Among the sediment-rich basal ice types, the temperate
382 dispersed basal ice from Matanuska Glacier contained approximately 6-fold more DNA per
383 gram of ice than the banded and solid basal ices from the cold-based Taylor Glacier (-15°C).
384 The concentration of extractable RNA was very low in all basal ice types (between 0.7 to
385 3.2 pg RNA g^{-1}; Table 2). The highest RNA concentration—though only marginally—was
386 observed in Matanuska Glacier's dispersed basal ice. These RNA concentrations were
387 consistent with ATP concentration data, a proxy for viable microbial biomass, and in
388 general, high concentrations of ATP g^{-1} ice were observed in sediment-rich basal ice types
389 versus those with low sediment content.

390 **3.3 Composition of microbial assemblages in different types of basal ice**

391 A total of 4,227,678 paired-end reads with an average read length of 253 bp were
392 obtained from MiSeq sequencing. After filtration and denoising, 2,883,221 non-chimeric
393 sequences representing 3,310 ASVs remained. Subsampling and culling of ASVs classified
394 as plastids or flagged as potential contaminants produced a final, curated dataset composed
395 of 2,005 ASVs.

396 Based on average-neighbor clustering of Bray-Curtis distances, the basal ice samples
397 clustered into three significantly different (AMOVA; $F[2,3]=5.23$, $p=0.017$) groups: (1)
398 Taylor Glacier sediment-poor basal ice, (2) Taylor Glacier sediment-rich basal ice, and (3)
399 Matanuska Glacier dispersed ice. The sediment-poor clean ice samples contained microbial
400 assemblages overwhelmingly composed of *Firmicutes* (68%) and *Proteobacteria* (25%),
401 with smaller proportions of *Bacteroidetes* (5%) and *Actinobacteria* (1%). The genus
402 *Tumebacillus* was especially abundant in the clean ice samples (Fig. 1A), representing more

403 than half of all taxa in these samples. Assemblages within the banded and solid ice samples
404 were comparatively more diverse than those found in clean ice (Fig. 2), with a wider range
405 of abundant phyla represented: *Actinobacteria* (26%), *Firmicutes* (23%), *Bacteroidetes*
406 (19%), *Proteobacteria* (11%), *Atribacteria* (9%), *Tenericutes* (7%), and *Planctomycetes*
407 (1%). Notably, ASVs related to the class *Clostridia* composed about 20% of the total in
408 these samples. The microbial assemblage within Matanuska's dispersed basal ice was
409 distinct from those observed from Taylor Glacier. Here we observed significant amounts of
410 *Nitrospirae* (39%) and *Betaproteobacteria* (30%), of which several of the most abundant
411 ASVs were related to sulfur and/or iron cycling members of the genera
412 *Thermodesulfovibrio*, *Rhodoferax*, and *Thiobacillus*. Comparing assemblages from all basal
413 ice samples, only 21 taxa (~3%) were shared between all four basal ice types (Table S1E).
414 These shared taxa were generally rare members with median relative abundances ranging
415 between 0.03% and 0.31%.

416 **3.4 Assessing metabolic status of bacterial taxa within different types of basal ice**

417 Of the 2,005 ASVs observed in this study, we detected 141 (7% of total) within the
418 RNA-derived 16S rRNA libraries (Table S1F), suggesting they were recovered from
419 potentially intact cells rather than eDNA or dead cells. From this group, 80 of the ASVs had
420 RNA/DNA abundance log-ratios >1 and likely represent metabolically active taxa within
421 the basal ice. The vast majority (63 ASVs) of these high-ratio ASVs were observed in the
422 dispersed ice from Matanuska Glacier (Fig. 1B), the warmest and youngest basal ice
423 sampled in this study. Many of the Matanuska Glacier ASVs were members of the
424 *Chloroflexi* and *Deltaproteobacteria,* with some of the largest RNA/DNA abundance log-
425 ratios belonging to *Desulfocapsa*, *Syntrophus*, and members of the family *Anaerolineaceae*.

426 Within the banded basal ice from Taylor Glacier, over half of ASVs detected in the RNA-
427 derived libraries were members of the *Firmicutes*. Among this phylum, members of the
428 *Paenisporosarcina*, *Paenibacillaceae*, *Desulfosporosinus*, *Caldicoprobacter*, and *Virgibacillus*
429 had the highest activity potential based on RNA/DNA abundance log-ratios (Table S1F) and
430 represented >90% of the RNA reads in these samples. In comparison, the clean and solid
431 basal ice samples contained the least number of potentially active members—10 ASVs from
432 only 472 RNA total reads, only 2 of which had RNA/DNA abundance log-ratios >1.

433 **3.5 Meta-Analysis: Microbial populations of various perennially frozen environments**

434 For the meta-analysis, we analyzed 54.6 million 16S rRNA sequences across 256
435 individual samples from 24 publicly available datasets that represent five different types of
436 freshwater ice environments: (1) supraglacial ice, (2) englacial ice, (3) basal ice, (4)
437 perennial cave ice, and (6) permafrost. After sequence filtering and curation, 7 samples
438 were excluded from meta-analysis due to low read depth. The final meta-analysis dataset
439 contained 25.7 million non-chimeric sequences representing 54,170 unique ASVs.
440 Subsampling to equal read depth reduced this to 35,357 ASVs.

441 We calculated Shannon diversity indices to compare microbial alpha diversity
442 between these frozen environments. Within the basal ice assemblages characterized in this
443 study, alpha diversity was significantly higher in the sediment-rich basal ice types than the
444 low sediment clean ices ($t(4)=3.34$, $p=0.03$) (Fig. 2). Compared to the other frozen
445 environments in the meta-analysis, alpha diversity within Antarctic sediment-rich basal ice
446 samples was most like that observed in basal ice from various coastal glaciers in Svalbard
447 (Tukey HSD mean difference = 0.07, p=1) (47). The lower alpha diversity values within
448 Taylor Glacier's clean ice were most like those found in englacial ice samples from the

449 GISP2D, NEEM, Guliya Ice Cap, and WAIS Divide ice cores (Tukey HSD mean difference =
450 0.39, p=1) (48–51).

451 To parameterize microbial β-diversity between samples, we used hierarchical
452 cluster analyses of both unweighted (UF) and weighted UniFrac (wUF) distances (Fig. 3 and
453 Fig. S4). In the UF cluster analysis (Fig. 3), microbial communities largely clustered by
454 environment type, indicating presence/absence data alone can reasonably discriminate
455 between different parts of the cryosphere. This suggests microbial community composition
456 in permanently frozen environments is strongly influenced by founder effects, possibly due
457 to a population bottleneck effect occurring upon freezing. In the cluster analysis of wUF,
458 the overall cluster pattern was comparable but many of the branching patterns between
459 samples were more statistically significant, indicating the inclusion of abundance data can
460 help discriminate samples from the same type of environment.

461 Within the cluster analyses, we also found some samples displayed larger variation
462 and overlap in community structures than others. For example, microbial assemblages
463 within englacial ice were the most similar (UF: 0.47 ± 0.15; mean ± s.d; n = 42). In contrast,
464 perennial cave ice samples (52, 53) had the highest heterogeneity among samples (UF: 0.85
465 ± 0.59; n=14). β-diversity of permafrost microbiomes were intermediate of these
466 endmembers, with relatively tight clustering observed in permafrost from the Storflaket
467 peat bog (northern Sweden) but wider variation in permafrost samples from University
468 Valley (Antarctica) (54, 55). The microbial communities within Taylor Glacier's banded and
469 solid basal ice facies clustered closely with perennial cave ices located in both Romania (52,
470 53) and California's Lava Bed National Monument (56). Those within the clean basal ice

471 were instead most similar to assemblages observed in englacial ice from the NEEM and
472 GISP2D ice cores from Greenland (48, 49)(Fig. 3).
473 We used an RDA model to determine how microbial lineages were distributed
474 across the different types of frozen environments (Fig. 4, left). The final RDA model
475 explained 50.7% of the variability between samples and effectively separated the samples
476 into three clusters, echoing patterns observed in the unifrac cluster analysis (Fig. 3). Of the
477 1627 microbial lineages included in the analysis, we identified 36 with loading vectors
478 greater than the equilibrium contribution (i.e., the proportion of variance that would be
479 explained by a random constrained axis), indicating they were associated with one or more
480 of the five types of frozen environments. Scalar projections of these lineages onto the
481 centroid factor of each type of frozen environment allowed us to estimate how strongly
482 these lineages were associated with each environment (Fig. 4, right). Unsurprisingly, many
483 supraglacial ice environments harbored comparatively higher proportions of
484 *Cyanobacteria* and plastid-harboring taxa than the other frozen environments. Englacial ice
485 environments were enriched with members of the genera *Pseudomonas*, *Methylobacterium*,
486 *Acinetobacter*, and *Polaromonas*, *Massilia,* and *Janthinobacterium*. In contrast, basal ice,
487 permafrost, and perennial cave ice environments all contained higher membership of
488 *Firmicutes* and *Actinobacteria* related taxa such as *Clostridium*, *Desulfosporosinus*,
489 *Oryzihumus*, and *Cryobacterium*.

490 **3.6 Meta-Analysis of early studies based on 16S rRNA clone sequencing**

491 Although 16S rRNA clone libraries lack the read depth to include in our primary
492 meta-analysis, we performed a secondary analysis to compare how many of the microbial
493 taxa observed in several early cryosphere microbiome studies (11, 57–60) compared to the

494 ‘indicator’ lineages we identified in Fig. 4. To achieve this, we inserted full-length clone
495 sequences into the meta-analysis reference tree using SEPP and taxonomically classified
496 them using Wang's Bayesian inference method with the Silva v.132 database as a reference.
497 Clone sequences were then agglomerated together with meta-analysis ASVs belonging to
498 the same genera.

499 Of the 236 16S rRNA clone sequences included in this secondary analysis, all but
500 three belonged to a taxon that had been observed in the meta-analysis. Despite their
501 extremely low read depth (between 11 and 136 clones), these five studies clustered with
502 similar environments in a distance-based RDA ordination (Fig. 5). Remarkably, of the 36
503 indicator taxa we identified in the primary meta-analysis, 12 were represented by at least
504 one clone sequence among these five studies. Many of these were among the most
505 abundant sequences observed in these clone libraries (Fig. S5).

506

507 **4. DISCUSSION**

508 **4.1 Microbial communities vary in size and composition across basal ice types**

509 Of the four different types of basal ice analyzed in this study, we found that those
510 containing large quantities of sediment or debris contained higher quantities of extractable
511 nucleic acids and microbial abundances than those containing low sediment content. This
512 is consistent with previous microbiological investigations of the GISP2 ice core that found
513 higher cell concentrations in the deepest sections of the core, where clay particles were
514 embedded in the basal ice (10). In addition to higher numbers of total cells and biomass,
515 microbial diversity is also notably higher in the sediment-rich basal ice facies relative to

516 clean basal ice or englacial ice, implicating subglacial debris as the primary source of
517 microorganisms in the basal ice.

518 Our estimates of bacterial cell abundance based on the yield of extracted DNA (~10^6
519 cells g^{-1} ice) were approximately 100-fold higher than those based on direct microscopic
520 counts (~10^4 cells g^{-1} ice) in the sediment-rich banded and solid basal ice. However, in the
521 clean basal ice samples, these estimates were highly comparable (Table 2). This difference
522 likely reflects the much greater efficiency of DNA extraction versus that of cell extraction. It
523 may also be related to the increased prevalence of eukaryotic genomes or environmental
524 DNA that is associated with sediment-rich basal ices (47, 61, 62). Alternatively, Taylor
525 Glacier's debris-rich basal ice may contain significant amounts of necromass. This would be
526 consistent with previous studies that have found some deep, debris-rich horizons of basal
527 ice, such as those of the Greenland ice sheet, contain ancient DNA from buried organisms
528 (63).

529 We found microbial assemblages within basal ices of the cold-based (-15°C) Taylor
530 Glacier to contain high abundances of *Firmicutes* and *Actinobacteria* relative to the other
531 frozen habitats examined. These Gram-positive phyla are commonly observed as the
532 dominant taxa in a wide range of frozen environments including ground ice, permafrost,
533 polar saline springs, cryopegs, and sea ice (60, 64–69). One possible explanation for these
534 high abundances is that the physiochemical stresses faced by cells under frozen conditions
535 (70) favor the prevalence of microorganisms that can form highly resistant endospores
536 (*Firmicutes*) or spores (*Actinobacteria*). Indeed, the ability to enter a metabolically dormant
537 state and form an environmentally resistant spore likely represents a robust survival
538 strategy for microorganisms that become entrapped inside ice for extended timeframes

539 (71). However, multiple lines of evidence indicate this hypothesis does not adequately
540 explain the abundance of these spore-forming taxa in our basal ice samples. First, ASVs
541 related to known endospore-forming genera such as *Paenisporosarcina*, *Virgibacillus*,
542 *Clostridium*, and *Desulfosporosinus* were abundant in all our RNA libraries. Because the
543 rRNA content of endospores decreases relatively quickly after sporulation—on the order of
544 days to weeks (72, 73)—their detection in >10,000-year-old basal ice implies these taxa
545 existed as vegetative cells and not as endospores within the ice. Second, populations of
546 *Paenisporosarcina* sp. isolated from the Taylor Glacier banded ice do not sporulate after
547 being refrozen in basal meltwater at in situ temperatures (-15°C), but instead continuously
548 incorporate radiolabeled DNA and protein precursors into macromolecules(3). Third, we
549 found pasteurization of banded basal ice meltwater dramatically reduced isolate
550 cultivability, indicating isolates were not being recovered from heat-resistant endospores.
551 Finally, 16S rRNA surveys of permafrost that have selectively depleted DNA from dead or
552 vegetative cells have found many endospore-forming taxa, especially members of the
553 *Clostridia*, were more likely to persist as vegetative cells rather than endospores in the
554 permafrost (74). Collectively, these results suggest the high abundances of *Firmicutes* and
555 *Actinobacteria* in Taylor Glacier's basal ice may not only be related to their environmental
556 durability while dormant, but also due to properties associated with their vegetative cycle
557 that promote physiological activities within frozen matrices (3).

558 **4.2 Young and warm versus old and cold basal ice**

559 Due to the chemical and biological lability of RNA, paired RNA/DNA 16S rRNA
560 amplicon libraries provide a useful proxy for discerning viable and metabolically active
561 microorganisms in a community from those that are dead or dormant. However, there are

limitations to this analysis and over interpretation of ratios as reliable indicators of relative metabolic activity of different ASVs should be viewed with caution (75). This may especially be the case in frozen environments, where RNA may be more stable in dormant cells. As such, we focus primarily on the number of detected taxa in each basal ice type, especially those with high RNA/DNA abundance log-ratios, which are difficult to explain in ancient ice samples without invoking metabolic activity.

On average, only about 2% of the total ASVs in each sample were also detected in the paired RNA library. This low proportion of overlap suggests that only a small fraction of the microorganisms preserved in the basal ice are potentially metabolically active within the ice matrix. The dispersed basal ice from Matanuska Glacier contained a much larger number of high-ratio ASVs than any of the basal ice facies recovered from Taylor Glacier (Fig. 1). One plausible explanation for this observation is the substantial difference in underlying geology, age, and temperature of basal ice between the two glaciers.

Assuming similar starting inputs of microbes, older ice would be expected to harbor smaller numbers of potentially active populations than younger ice due to microbial attrition over time (70). Analysis of the δD and $\delta^{18}O$ composition of meltwater from Taylor Glacier surface ice samples estimate ages of 11,500 to 65,000 years BP (76), while recent radiometric ^{81}Kr dating efforts have yielded age estimates near the glacial terminus of 123,500 years BP (77). In comparison, measurements of oxygen isotopes in Matanuska Glacier's dispersed basal ice layer indicated the basal ice originated in the accumulation area (78). Based on the velocity of Matanuska Glacier (~110 m yr^{-1}), this would represent an approximate time of 250 years between deposition and terminal ablation. Trace amounts of anthropogenic tritium produced by atmospheric thermonuclear weapon tests

in the 1950s and 1960s have also been detected in Matanuska Glacier's basal ice zone (79), indicating portions of this ice were formed even more recently by freeze-on of surface-derived meltwater (80). This indicates the dispersed ice we sampled from Matanuska is substantially younger than any of the basal ice types collected from Taylor Glacier, with the latter probably being between ~100- to 500-times older than the former.

In addition to age of the basal ice, the large difference in ice temperature between a temperate and cold-based glacier would also affect the potential for metabolic activity in the ice habitat (19, 81). Taylor Glacier is a cold-based glacier with a basal ice temperature of -15°C (4). In contrast, the Matanuska Glacier is temperate, and the basal ice zone is at the pressure melting point of 0°C (82). As such, cells present in the liquid habitat at grain boundaries (81) in Taylor Glacier's basal ice are under considerably higher physiochemical stress than ice near the melting point. For example, the predicted ionic strength of the briny liquid at ice crystal boundaries—where the microorganisms are located— is nearly 4.6M at -15°C. Comparatively, this is 11.5-fold higher than estimates for unfrozen water in glacial ice at -1°C (70). Hence, the wider diversity and increased number of ASVs with a high potential for metabolic activity in the dispersed basal ice may reflect not only the sample age, but the more favorable conditions for metabolism in temperate versus cold-based glacial ice matrices.

4.3 Debris-rich basal ice types are hot spots for microbial activity

Multiple studies have reported observations of very low concentrations of oxygen (17) and large excesses of CH_4 in debris-rich basal ice from the Greenland and Antarctica ice sheets (10, 30, 83–86). Mirroring these findings, an analysis of gasses entrapped within Taylor Glacier banded basal ice found O_2 was depleted to as low as 4% in horizons where

608 CO_2 concentrations were concurrently enriched as high as 20,000-fold relative to
609 atmospheric concentrations (4). Isotopic analysis of $\delta^{13}C$-CO_2 revealed this CO_2 was
610 isotopically depleted (-24‰), and therefore, was likely produced by microbial respiration
611 of organic matter (87). In this study, among all the RNA-based 16S rRNA libraries we
612 sequenced from Taylor Glacier basal ice, we found the largest reads counts and largest
613 number of potentially active ASVs in these same banded basal ice horizons. Together with
614 elevated ATP concentrations, these observations collectively suggest Taylor Glacier's
615 banded basal ice horizons harbor metabolically active microbiomes that alter entrapped
616 gas compositions by actively metabolizing organic matter to CO_2 at -15°C within the ice
617 matrix.

618 Alternatively, these trends in gas data could be the result of microbial activity that
619 had occurred before the basal ice formed. One way to explore this possibility is by
620 considering the total gas content of the ice. If the gases were dissolved in the water that
621 froze onto the base of the glacier, then total gas volumes as low as 0.02 to 0.08 cc/g would
622 be expected (88, 89). In solid facies of the Taylor Glacier basal ice profile, the lower total
623 gas volumes observed were indeed low (0.01 to 0.07 cc/g; (4)). Hence, although we did not
624 see much evidence for microbial activity in the solid basal ice, we cannot exclude largescale
625 melting/refreezing processes occurred during its formation. In contrast, in the banded
626 basal ice—where isotopic, ATP, and RNA data provided strong evidence for microbial
627 activity—the total gas volumes were consistent with those observed in the clean ice (0.09
628 to 0.11 cc/g; (4)). These volumes are more similar to those typically seen in englacial ice of
629 meteoric origin (0.1 cc/g; (90)). In summary, large-scale melting/refreezing cannot explain

the gas data observed across all facies, and in the banded ice, in situ microbial respiration is the only explanation consistent with its total gas content.

This metabolic activity may simply be a consequence of substrate availability for microbial consumption. Previous geochemical analysis of Taylor Glacier's basal ice found dissolved organic carbon (DOC) concentrations are much higher in the debris-rich basal ice types (~63 mg L^{-1}) than in the debris-poor types (~0.8 mg L^{-1}; (4, 87)) However, our comparison of multiple basal ice types suggests there are likely additional, unidentified factors besides sediment content controlling whether basal ice harbors an active microbiome. For example, although the banded and solid basal ice samples harbored very similar microbial communities in our DNA-based libraries, we found very little evidence for active ASVs within the solid basal ice. This suggests—at least in polar glaciers containing basal ice horizons well below 0°C—elevated debris and/or DOC are not alone sufficient for supporting metabolic activity in the ice.

In many of the debris-rich basal ice types we investigated in this study, we observed an enrichment of putatively anaerobic taxa (e.g., *Clostridia*) within the same samples where O_2 concentrations were depleted relative to atmospheric values. One possible explanation is that the subglacial debris within these horizons were enriched with these taxa before being entrained into the basal ice. Alternatively, these patterns represent ecological shifts in microbial community composition that occur inside the ice matrix as oxygen becomes depleted. However, there is an important nuance to how these shifts probably occur. Although there is ample evidence that some microbial taxa can remain metabolically active while frozen (3, 91–94), there is comparatively little concrete evidence that microorganisms can physically grow and divide while frozen inside ice. This suggests that

reproduction does not occur, and if it does, is imperceptibly slow under the conditions within an ice matrix. Hence, the increased relative abundance of many putative anaerobic taxa that we observed in many of the sediment rich basal ice samples likely represents a decline of strictly aerobic taxa after oxygen has become depleted rather than a genuine enrichment or outgrowth of putative anaerobes. This hypothesis may explain why enrichment cultures inoculated with 100,000-year-old Greenland basal ice became turbid substantially faster (2 to 3 weeks versus several months) when incubated anaerobically versus aerobically (95).

4.4. Basal ice diagenesis likely controls microbiome composition and structure

The microbiomes of cold-based, debris-rich basal ice horizons such as the banded and solid basal ice from Taylor Glacier were phylogenetically most like those in perennial cave ice or permafrost. These similarities are likely a reflection of the comparable physiochemical conditions found within these environments. All three are characterized by relatively high concentrations of debris, constant subzero temperatures, and perhaps—as suggested by the co-enrichment of several putative anaerobic taxa (e.g., *Clostridium*, *Desulfosporosinus*) in some samples—depleted or decreased oxygen concentrations. In contrast, clean basal ice appears to harbor microbiomes most like those found in englacial ice. This is consistent with the notion that clean basal ice and englacial ice are diagenetically very similar. Both contain very little to no debris and are typically formed from the accumulation and compression of snow into glacial ice. In fact, except in unique cases where new clean basal ice is formed by the accretion of subglacial lake water onto the base of a glacier, the only real difference between clean basal and englacial ice may be location. In other words, in many cases clean basal ice is simply deep englacial ice.

676 Collectively, these findings suggest the microbiomes of basal ice environments are not
677 simply preserved communities but rather are actively structured by the diagenesis and
678 physiochemical nature of their habitat.

679 **4.5 Meta-analysis limitations**

680 Comparing 16S rRNA amplicon datasets from different studies is hindered by
681 inconsistencies in the sequencing platform used and the variable region of the 16S rRNA
682 gene that was amplified for sequencing. Using SEPP, heterogeneous ASVs from different
683 studies are inserted into the same reference tree. This creates stable phylogenetic
684 placements that enable integration and meta-analysis of amplicon data from multiple
685 variable regions of the 16S rRNA gene (34). Nevertheless, it is important to note the
686 limitations of this approach. First, integrating previously published 16S rRNA amplicon
687 datasets based on DGGE profiling remains difficult as they lack sufficient read depth or
688 taxonomic resolution to make meaningful comparisons with more modern datasets. As a
689 result, our meta-analysis excluded many of the pioneering works that investigated the
690 microbial ecology of glacial ice. Second, there are potential biases in our meta-analysis due
691 to how we classified some icy environments. For example, while it is clear supraglacial ice
692 exists on the surface, there is no universal definition of a depth wherein glacial ice should
693 suddenly be considered 'englacial'. Indeed, supraglacial and englacial ice would probably
694 be more accurately portrayed as opposite ends of a vertical gradient through the body of a
695 glacier rather than discrete categories. This may explain some of the overlap in microbiome
696 composition and structure we observed between supraglacial and englacial environments
697 (Figs. 4 and 5).

Another potential source of bias in the meta-analysis to be cognizant of is how some ice samples are collected, specifically basal ice. Due to the logistical difficulty of accessing the basal ice zone of a glacier, most samples of basal ice included in the meta-analysis were not collected from inside an excavated tunnel like our samples at Taylor Glacier. Instead, most of these samples (including our sample of Matanuska's dispersed basal ice), were collected from easily accessible horizons of basal ice that were exposed at the glacial margin. These samples have been exposed to sunlight and seasonal temperature fluctuations that are not found in the glacial interior. It is difficult to accurately predict how these conditions would affect the basal ice microbiomes. However, it might explain why, for example, phototrophic taxa (e.g., *Cyanobacteria*) are observed in several of the basal ice samples from coastal Svalbard glaciers.

4.6 Conclusions and Implications

Our findings show that certain microbes do not persist in a state of dormancy while frozen, and coupled with other biogeochemical data (3, 4), indicate that the sediment-rich basal ice horizons of glaciers harbor microbial communities that actively conduct biogeochemical cycling at subzero temperatures. Although we have limited observations, our data further implies that a larger diversity of bacteria remain metabolically active in temperate basal ice found beneath nonpolar glaciers and ice sheet interiors (82, 96). Given that the basal temperature of the Antarctic and Greenland ice sheets are near or at the pressure-melting point (97), this raises the intriguing possibility that subglacial regions of the cryosphere may be more biogeochemically active than previously thought.

Microorganisms in the basal ice of cold-based glaciers may be important biogeochemical actors. Although rates of microbial activity in these environments are

extremely low and much lower than those of warmer environments (3, 36, 91, 98, 99), this may be offset by the long residence time of basal ice. Microbial processing in basal ice could have important implications to material that is transported to and melts at the margin, representing an important source of dissolved organic carbon, nutrients, and trace metals to marine ecosystems (23, 26, 100, 101).

Finally, our meta-analysis demonstrates that basal ice environments harbor a diverse range of microbial communities which can resemble those found in a wide range of other icy environments. This is likely a reflection of the many different types of basal ice, which vary considerable in both physical and chemical characteristics (46). Debris-rich basal ice types, with comparatively higher concentrations of potential nutrients and redox substrates for microbial metabolism resemble other debris-rich icy environments such as permafrost and/or perennial cave ice. Likewise, clean basal ice microbial communities are more like those found in the oligotrophic, debris-free englacial ice that makes up the bulk of a glacier's mass. Broadly, these findings indicate basal ice diagenesis plays a major role in microbiome composition and structure.

5. ACKNOWLEDGEMENTS

This study was funded by a Division of Polar Programs grant (ANT-0636828) from the National Science Foundation. We thank Amanda Achberger, Pierre Amato, Tim Brox, Lindsay Knippenberg, Scott Montross, and Mark Skidmore for multiple discussions and as vital partners in tunnel excavation and sampling in Antarctica. We also thank the staff of McMurdo station and Petroleum Helicopters International for logistical support in the field.

6. REFERENCES

1. Knight PG. 1997. The basal ice layer of glaciers and ice sheets. Quaternary Science Reviews 16:975–993.
2. Souchez R, Jouzel J, Landais A, Chappellaz J, Lorrain R, Tison J-L. 2006. Gas isotopes in ice reveal a vegetated central Greenland during ice sheet invasion. Geophysical Research Letters 33.
3. Doyle S, Montross S, Skidmore M, Christner B. 2013. Characterizing Microbial Diversity and the Potential for Metabolic Function at −15 °C in the Basal Ice of Taylor Glacier, Antarctica. Biology 2:1034–1053.
4. Montross S, Skidmore M, Christner B, Samyn D, Tison J-L, Lorrain R, Doyle S, Fitzsimons S. 2014. Debris-Rich Basal Ice as a Microbial Habitat, Taylor Glacier, Antarctica. Geomicrobiology Journal 31:76–81.
5. Siegert MJ, Ellis-Evans JC, Tranter M, Mayer C, Petit J-R, Salamatin A, Priscu JC. 2001. Physical, chemical and biological processes in Lake Vostok and other Antarctic subglacial lakes. 6864. Nature 414:603–609.
6. Achberger AM, Michaud AB, Vick-Majors TJ, Christner BC, Skidmore ML, Priscu JC, Tranter M. 2017. Microbiology of subglacial environments, p. 83–110. *In* Psychrophiles: from biodiversity to biotechnology. Springer.
7. Samyn D, Svensson A, Fitzsimons SJ. 2008. Dynamic implications of discontinuous recrystallization in cold basal ice: Taylor Glacier, Antarctica. Journal of Geophysical Research 113.
8. Skidmore ML, Foght JM, Sharp MJ. 2000. Microbial Life beneath a High Arctic Glacier. Appl Environ Microbiol 66:3214–3220.

9. Wadham JL, Bottrell S, Tranter M, Raiswell R. 2004. Stable isotope evidence for microbial sulphate reduction at the bed of a polythermal high Arctic glacier. Earth and Planetary Science Letters 219:341–355.

10. Tung H c., Price P b., Bramall N e., Vrdoljak G. 2006. Microorganisms Metabolizing on Clay Grains in 3-Km-Deep Greenland Basal Ice. Astrobiology 6:69–86.

11. Yde JC, Finster KW, Raiswell R, Steffensen JP, Heinemeier J, Olsen J, Gunnlaugsson HP, Nielsen OB. 2010. Basal ice microbiology at the margin of the Greenland ice sheet. Annals of Glaciology 51:71–79.

12. Montross SN, Skidmore M, Tranter M, Kivimaki A-L, Parkes RJ. 2013. A microbial driver of chemical weathering in glaciated systems. Geology 41:215–218.

13. Bunt J. 1963. Microbiology of Antarctic sea-ice: diatoms of Antarctic sea-ice as agents of primary production. Nature 199:1255–1257.

14. Abyzov S, Mitskevich I, Poglazova M. 1998. The Microflora of Deep Horizons of the Central Antarctic Ice Sheet. Mikrobiologiya 67:547–555.

15. Sowers T. 2001. N2O record spanning the penultimate deglaciation from the Vostok ice core. Journal of Geophysical Research: Atmospheres 106:31903–31914.

16. Campen RK, Sowers T, Alley RB. 2003. Evidence of microbial consortia metabolizing within a low-latitude mountain glacier. Geology 31:231.

17. Souchez R, Janssens L, Lemmens M, Stauffer B. 1995. Very low oxygen concentration in basal ice from Summit, central Greenland. Geophysical Research Letters 22:2001–2004.

18. Souchez R, Bouzette A, Clausen HB, Johnsen SJ, Jouzel J. 1998. A stacked mixing sequence at the base of the Dye 3 Core, Greenland. Geophysical Research Letters 25:1943–1946.

19. Price PB, Sowers T. 2004. Temperature dependence of metabolic rates for microbial growth, maintenance, and survival. PNAS 101:4631–4636.

20. Wadham JL, Tranter M, Skidmore M, Hodson AJ, Priscu J, Lyons WB, Sharp M, Wynn P, Jackson M. 2010. Biogeochemical weathering under ice: Size matters: GLACIAL BIOGEOCHEMICAL WEATHERING. Global Biogeochemical Cycles 24:n/a-n/a.

21. Barker JD, Grottoli AG, Lyons WB. 2018. Stable isotope evidence for the biogeochemical transformation of ancient organic matter beneath Suess Glacier, Antarctica. Arctic, Antarctic, and Alpine Research 50:e1448643.

22. Hopwood MJ, Carroll D, Dunse T, Hodson A, Holding JM, Iriarte JL, Ribeiro S, Achterberg EP, Cantoni C, Carlson DF, Chierici M, Clarke JS, Cozzi S, Fransson A, Juul-Pedersen T, Winding MS, Meire L. 2019. Review Article: How does glacier discharge affect marine biogeochemistry and primary production in the Arctic? The Cryosphere Discussions 1–51.

23. Vick-Majors TJ, Michaud AB, Skidmore ML, Turetta C, Barbante C, Christner BC, Dore JE, Christianson K, Mitchell AC, Achberger AM, Mikucki JA, Priscu JC. 2020. Biogeochemical Connectivity Between Freshwater Ecosystems beneath the West Antarctic Ice Sheet and the Sub-Ice Marine Environment. Global Biogeochemical Cycles 34:e2019GB006446.

24. Hood E, Fellman J, Spencer RGM, Hernes PJ, Edwards R, D'Amore D, Scott D. 2009. Glaciers as a source of ancient and labile organic matter to the marine environment. 7276. Nature 462:1044–1047.

25. Bhatia MP, Das SB, Xu L, Charette MA, Wadham JL, Kujawinski EB. 2013. Organic carbon export from the Greenland ice sheet. Geochimica et Cosmochimica Acta 109:329–344.

26. Hawkings JR, Skidmore ML, Wadham JL, Priscu JC, Morton PL, Hatton JE, Gardner CB, Kohler TJ, Stibal M, Bagshaw EA, Steigmeyer A, Barker J, Dore JE, Lyons WB, Tranter M, Spencer RGM, Team the SS. 2020. Enhanced trace element mobilization by Earth's ice sheets. PNAS 117:31648–31659.

27. Priscu JC, Tulaczyk S, Studinger M, Kennicutt M, Christner BC, Foreman CM. 2008. Antarctic subglacial water: origin, evolution and ecology. Polar lakes and rivers: limnology of Arctic and Antarctic aquatic ecosystems Oxford University Press, Oxford 119–135.

28. Batjes NH. 2014. Total carbon and nitrogen in the soils of the world. European Journal of Soil Science 65:10–21.

29. Wadham JL, Tranter M, Tulaczyk S, Sharp M. 2008. Subglacial methanogenesis: A potential climatic amplifier? Global Biogeochemical Cycles 22.

30. Wadham JL, Arndt S, Tulaczyk S, Stibal M, Tranter M, Telling J, Lis GP, Lawson E, Ridgwell A, Dubnick A, Sharp MJ, Anesio AM, Butler CEH. 2012. Potential methane reservoirs beneath Antarctica. Nature 488:633–637.

830 31. Boyd ES, Skidmore M, Mitchell AC, Bakermans C, Peters JW. 2010. Methanogenesis
831 in subglacial sediments: Subglacial methanogenesis. Environmental Microbiology
832 Reports 2:685–692.
833 32. Dieser M, Broemsen ELJE, Cameron KA, King GM, Achberger A, Choquette K,
834 Hagedorn B, Sletten R, Junge K, Christner BC. 2014. Molecular and biogeochemical
835 evidence for methane cycling beneath the western margin of the Greenland Ice
836 Sheet. The ISME Journal 8:2305–2316.
837 33. Michaud AB, Dore JE, Achberger AM, Christner BC, Mitchell AC, Skidmore ML, Vick-
838 Majors TJ, Priscu JC. 2017. Microbial oxidation as a methane sink beneath the West
839 Antarctic Ice Sheet. 8. Nature Geoscience 10:582–586.
840 34. Janssen S, McDonald D, Gonzalez A, Navas-Molina JA, Jiang L, Xu ZZ, Winker K, Kado
841 DM, Orwoll E, Manary M, Mirarab S, Knight R. 2018. Phylogenetic Placement of Exact
842 Amplicon Sequences Improves Associations with Clinical Information. mSystems
843 3:e00021-18.
844 35. Christner BC, Mikucki JA, Foreman CM, Denson J, Priscu JC. 2005. Glacial ice cores: A
845 model system for developing extraterrestrial decontamination protocols. Icarus
846 174:572–584.
847 36. Amato P, Christner BC. 2009. Energy Metabolism Response to Low-Temperature
848 and Frozen Conditions in Psychrobacter cryohalolentis. Applied and Environmental
849 Microbiology 75:711–718.
850 37. Caporaso JG, Lauber CL, Walters WA, Berg-Lyons D, Huntley J, Fierer N, Owens SM,
851 Betley J, Fraser L, Bauer M, others. 2012. Ultra-high-throughput microbial

852 community analysis on the Illumina HiSeq and MiSeq platforms. The ISME journal
853 6:1621–1624.
854 38. Salter SJ, Cox MJ, Turek EM, Calus ST, Cookson WO, Moffatt MF, Turner P, Parkhill J,
855 Loman NJ, Walker AW. 2014. Reagent and laboratory contamination can critically
856 impact sequence-based microbiome analyses. BMC biology 12:87.
857 39. Eisenhofer R, Minich JJ, Marotz C, Cooper A, Knight R, Weyrich LS. 2019.
858 Contamination in Low Microbial Biomass Microbiome Studies: Issues and
859 Recommendations. Trends in Microbiology 27:105–117.
860 40. Callahan BJ, McMurdie PJ, Rosen MJ, Han AW, Johnson AJA, Holmes SP. 2016.
861 DADA2: High-resolution sample inference from Illumina amplicon data. Nature
862 Methods 13:581–583.
863 41. Wang Q, Garrity GM, Tiedje JM, Cole JR. 2007. Naïve Bayesian Classifier for Rapid
864 Assignment of rRNA Sequences into the New Bacterial Taxonomy. Appl Environ
865 Microbiol 73:5261–5267.
866 42. Quast C, Pruesse E, Yilmaz P, Gerken J, Schweer T, Yarza P, Peplies J, Glockner FO.
867 2013. The SILVA ribosomal RNA gene database project: improved data processing
868 and web-based tools. Nucleic Acids Research 41:D590–D596.
869 43. McDonald D, Price MN, Goodrich J, Nawrocki EP, DeSantis TZ, Probst A, Andersen
870 GL, Knight R, Hugenholtz P. 2012. An improved Greengenes taxonomy with explicit
871 ranks for ecological and evolutionary analyses of bacteria and archaea. The ISME
872 journal 6:610.
873 44. Mirarab S, Nguyen N, Warnow T. 2012. SEPP: SATé-enabled phylogenetic placement,
874 p. 247–258. *In* Biocomputing 2012. World Scientific.

875 45. Kimes PK, Liu Y, Neil Hayes D, Marron JS. 2017. Statistical significance for
876 hierarchical clustering. Biometrics 73:811–821.
877 46. Hubbard B, Cook S, Coulson H. 2009. Basal ice facies: a review and unifying
878 approach. Quaternary Science Reviews 28:1956–1969.
879 47. Perini L, Gostinčar C, Gunde-Cimerman N. 2019. Fungal and bacterial diversity of
880 Svalbard subglacial ice. 1. Scientific Reports 9:20230.
881 48. Miteva V, Rinehold K, Sowers T, Sebastian A, Brenchley J. 2015. Abundance, viability
882 and diversity of the indigenous microbial populations at different depths of the
883 NEEM Greenland ice core. Polar Research 34:25057.
884 49. Miteva V, Sowers T, Schüpbach S, Fischer H, Brenchley J. 2016. Geochemical and
885 Microbiological Studies of Nitrous Oxide Variations within the New NEEM
886 Greenland Ice Core during the Last Glacial Period. Geomicrobiology Journal 33:647–
887 660.
888 50. Price PB, Morris J, Bay RC, Adhikari A, Giovannoni SJ, Vergin KL. 2015. Molecular
889 Fossils from Microorganisms Preserved in Glacial Ice. bioRxiv
890 https://doi.org/10.1101/019240.
891 51. Zhong Z-P, Tian F, Roux S, Gazitúa MC, Solonenko NE, Li Y-F, Davis ME, Van Etten JL,
892 Mosley-Thompson E, Rich VI, Sullivan MB, Thompson LG. 2021. Glacier ice archives
893 nearly 15,000-year-old microbes and phages. Microbiome 9:160.
894 52. Itcus C, Pascu MD, Lavin P, Perşoiu A, Iancu L, Purcarea C. 2018. Bacterial and
895 archaeal community structures in perennial cave ice. Sci Rep 8.
896 53. Paun VI, Icaza G, Lavin P, Marin C, Tudorache A, Perşoiu A, Dorador C, Purcarea C.
897 2019. Total and Potentially Active Bacterial Communities Entrapped in a Late

898 Glacial Through Holocene Ice Core From Scarisoara Ice Cave, Romania. Frontiers in
899 Microbiology 10:1193.
900 54. Goordial J, Davila A, Lacelle D, Pollard W, Marinova MM, Greer CW, DiRuggiero J,
901 McKay CP, Whyte LG. 2016. Nearing the cold-arid limits of microbial life in
902 permafrost of an upper dry valley, Antarctica. 7. The ISME Journal 10:1613–1624.
903 55. Monteux S, Weedon JT, Blume-Werry G, Gavazov K, Jassey VEJ, Johansson M, Keuper
904 F, Olid C, Dorrepaal E. 2018. Long-term in situ permafrost thaw effects on bacterial
905 communities and potential aerobic respiration. The ISME Journal 12:2129–2141.
906 56. O'Connor BRW, Fernández-Martínez MÁ, Léveillé RJ, Whyte LG. 2021. Taxonomic
907 Characterization and Microbial Activity Determination of Cold-Adapted Microbial
908 Communities in Lava Tube Ice Caves from Lava Beds National Monument, a High-
909 Fidelity Mars Analogue Environment. Astrobiology 21:613–627.
910 57. Skidmore M, Anderson SP, Sharp M, Foght J, Lanoil BD. 2005. Comparison of
911 Microbial Community Compositions of Two Subglacial Environments Reveals a
912 Possible Role for Microbes in Chemical Weathering Processes. Applied and
913 Environmental Microbiology 71:6986–6997.
914 58. Cheng SM, Foght JM. 2007. Cultivation-independent and -dependent
915 characterization of Bacteria resident beneath John Evans Glacier: Characterization
916 of subglacial Bacterial communities. FEMS Microbiology Ecology 59:318–330.
917 59. Katayama T, Tanaka M, Moriizumi J, Nakamura T, Brouchkov A, Douglas TA, Fukuda
918 M, Tomita F, Asano K. 2007. Phylogenetic Analysis of Bacteria Preserved in a
919 Permafrost Ice Wedge for 25,000 Years. Applied and Environmental Microbiology
920 73:2360–2363.

921 60. Steven B, Pollard WH, Greer CW, Whyte LG. 2008. Microbial diversity and activity
922 through a permafrost/ground ice core profile from the Canadian high Arctic.
923 Environmental Microbiology 10:3388–3403.
924 61. Sonjak S, Frisvad JC, Gunde-Cimerman N. 2006. Penicillium Mycobiota in Arctic
925 Subglacial Ice. Microbial Ecology 52:207–216.
926 62. Fraser CI, Connell L, Lee CK, Cary SC. 2018. Evidence of plant and animal
927 communities at exposed and subglacial (cave) geothermal sites in Antarctica. Polar
928 Biol 41:417–421.
929 63. Willerslev E, Cappellini E, Boomsma W, Nielsen R, Hebsgaard MB, Brand TB,
930 Hofreiter M, Bunce M, Poinar HN, Dahl-Jensen D, Johnsen S, Steffensen JP, Bennike O,
931 Schwenninger J-L, Nathan R, Armitage S, de Hoog C-J, Alfimov V, Christl M, Beer J,
932 Muscheler R, Barker J, Sharp M, Penkman KEH, Haile J, Taberlet P, Gilbert MTP,
933 Casoli A, Campani E, Collins MJ. 2007. Ancient Biomolecules from Deep Ice Cores
934 Reveal a Forested Southern Greenland. Science 317:111–114.
935 64. Kochkina G, Ivanushkina N, Karasev S, Gavrish EY, Gurina L, Evtushenko L, Spirina E,
936 Vorob'eva E, Gilichinskii D, Ozerskaya S. 2001. Survival of micromycetes and
937 actinobacteria under conditions of long-term natural cryopreservation.
938 Microbiology 70:356–364.
939 65. Steven B, Briggs G, McKay CP, Pollard WH, Greer CW, Whyte LG. 2007.
940 Characterization of the microbial diversity in a permafrost sample from the
941 Canadian high Arctic using culture-dependent and culture-independent methods:
942 Microbial diversity in Canadian high Arctic permafrost. FEMS Microbiology Ecology
943 59:513–523.

944 66. Perreault NN, Greer CW, Andersen DT, Tille S, Lacrampe-Couloume G, Lollar BS,
945 Whyte LG. 2008. Heterotrophic and Autotrophic Microbial Populations in Cold
946 Perennial Springs of the High Arctic. Appl Environ Microbiol 74:6898–6907.
947 67. Lacelle D, Radtke K, Clark ID, Fisher D, Lauriol B, Utting N, Whyte LG. 2011.
948 Geomicrobiology and occluded O2–CO2–Ar gas analyses provide evidence of
949 microbial respiration in ancient terrestrial ground ice. Earth and Planetary Science
950 Letters 306:46–54.
951 68. Boetius A, Anesio AM, Deming JW, Mikucki JA, Rapp JZ. 2015. Microbial ecology of
952 the cryosphere: sea ice and glacial habitats. 11. Nature Reviews Microbiology
953 13:677–690.
954 69. Spirina E, Durdenko E, Demidov N, Abramov A, Romanovsky V, Rivkina E. 2017.
955 Halophilic-psychrotrophic bacteria of an Alaskan cryopeg—a model for
956 astrobiology. Paleontological Journal 51:1440–1452.
957 70. Doyle S, Dieser M, Broemsen E, Christner B. 2012. General characteristics of cold-
958 adapted microorganisms, p. 103–125. *In* Polar Microbiology: Life in a Deep Freeze.
959 American Society of Microbiology.
960 71. Filippidou S, Wunderlin T, Junier T, Jeanneret N, Dorador C, Molina V, Johnson DR,
961 Junier P. 2016. A Combination of Extreme Environmental Conditions Favor the
962 Prevalence of Endospore-Forming Firmicutes. Front Microbiol 7.
963 72. Segev E, Smith Y, Ben-Yehuda S. 2012. RNA Dynamics in Aging Bacterial Spores. Cell
964 148:139–149.
965 73. Korza G, Setlow B, Rao L, Li Q, Setlow P. 2016. Changes in Bacillus Spore Small
966 Molecules, rRNA, Germination, and Outgrowth after Extended Sublethal Exposure to

Various Temperatures: Evidence that Protein Synthesis Is Not Essential for Spore Germination. J Bacteriol 198:3254–3264.

74. Burkert A, Douglas TA, Waldrop MP, Mackelprang R. 2019. Changes in the Active, Dead, and Dormant Microbial Community Structure across a Pleistocene Permafrost Chronosequence. Appl Environ Microbiol 85:e02646-18.

75. Blazewicz SJ, Barnard RL, Daly RA, Firestone MK. 2013. Evaluating rRNA as an indicator of microbial activity in environmental communities: limitations and uses. 11. The ISME Journal 7:2061–2068.

76. Aciego SM, Cuffey KM, Kavanaugh JL, Morse DL, Severinghaus JP. 2007. Pleistocene ice and paleo-strain rates at Taylor Glacier, Antarctica. Quaternary Research 68:303–313.

77. Buizert C, Baggenstos D, Jiang W, Purtschert R, Petrenko VV, Lu Z-T, Müller P, Kuhl T, Lee J, Severinghaus JP, others. 2014. Radiometric 81Kr dating identifies 120,000-year-old ice at Taylor Glacier, Antarctica. Proceedings of the National Academy of Sciences 111:6876–6881.

78. Lawson DE, Kulla JB. 1978. An Oxygen Isotope Investigation of the Origin of the Basal Zone of the Matanuska Glacier, Alaska. The Journal of Geology 86:673–685.

79. Strasser JC, Lawson DE, Larson GJ, Evenson EB, Alley RB. 1996. Preliminary results of tritium analyses in basal ice, Matanuska Glacier, Alaska, U.S.A.: evidence for subglacial ice accretion. Annals of Glaciology 22:126–133.

80. Lawson D. 1979. Sedimentological Analysis of the Western Terminus Region of the Matanuska Glacier, Alaska 132.

81. Price PB. 2000. A habitat for psychrophiles in deep Antarctic ice. PNAS 97:1247–1251.

82. Lawson DE, Strasser JC, Evenson EB, Alley RB, Larson GJ, Arcone SA. 1998. Glaciohydraulic supercooling: a freeze-on mechanism to create stratified, debris-rich basal ice: I. Field evidence. Journal of Glaciology 44:547–562.

83. Rhodes RH, Faïn X, Stowasser C, Blunier T, Chappellaz J, McConnell JR, Romanini D, Mitchell LE, Brook EJ. 2013. Continuous methane measurements from a late Holocene Greenland ice core: Atmospheric and in-situ signals. Earth and Planetary Science Letters 368:9–19.

84. Lamarche-Gagnon G, Wadham JL, Sherwood Lollar B, Arndt S, Fietzek P, Beaton AD, Tedstone AJ, Telling J, Bagshaw EA, Hawkings JR, Kohler TJ, Zarsky JD, Mowlem MC, Anesio AM, Stibal M. 2019. Greenland melt drives continuous export of methane from the ice-sheet bed. 7737. Nature 565:73–77.

85. Lee JE, Edwards JS, Schmitt J, Fischer H, Bock M, Brook EJ. 2020. Excess methane in Greenland ice cores associated with high dust concentrations. Geochimica et Cosmochimica Acta 270:409–430.

86. Stibal M, Wadham JL, Lis GP, Telling J, Pancost RD, Dubnick A, Sharp MJ, Lawson EC, Butler CEH, Hasan F, Tranter M, Anesio AM. 2012. Methanogenic potential of Arctic and Antarctic subglacial environments with contrasting organic carbon sources. Global Change Biology 18:3332–3345.

87. Montross SN. 2012. Biogeochemistry of basal ice from Taylor Glacier, Antarctica. Montana State University.

1011 88. Cuffey KM, Conway H, Gades AM, Hallet B, Lorrain R, Severinghaus JP, Steig EJ,
1012 Vaughn B, White JWC. 2000. Entrainment at cold glacier beds. Geology 28:351–354.
1013 89. Sleewaegen S, Samyn D, Fitzsimons SJ, Lorrain RD. 2003. Equifinality of basal ice
1014 facies from an Antarctic cold-based glacier. Annals of Glaciology 37:257–262.
1015 90. Paterson WSB. 1994. Physics of glaciers. Butterworth-Heinemann.
1016 91. Panikov NS, Flanagan PW, Oechel WC, Mastepanov MA, Christensen TR. 2006.
1017 Microbial activity in soils frozen to below −39°C. Soil Biology and Biochemistry
1018 38:785–794.
1019 92. Bakermans C, Skidmore ML. 2011. Microbial Metabolism in Ice and Brine at −5°C:
1020 Microbial metabolism in ice and brine at −5°C. Environmental Microbiology
1021 13:2269–2278.
1022 93. Tuorto SJ, Darias P, McGuinness LR, Panikov N, Zhang T, Häggblom MM, Kerkhof LJ.
1023 2014. Bacterial genome replication at subzero temperatures in permafrost. ISME J
1024 8:139–149.
1025 94. Segura JH, Nilsson MB, Haei M, Sparrman T, Mikkola J-P, Gräsvik J, Schleucher J,
1026 Öquist MG. 2017. Microbial mineralization of cellulose in frozen soils. Nat Commun
1027 8:1154.
1028 95. Sheridan PP, Miteva VI, Brenchley JE. 2003. Phylogenetic Analysis of Anaerobic
1029 Psychrophilic Enrichment Cultures Obtained from a Greenland Glacier Ice Core.
1030 Applied and Environmental Microbiology 69:2153–2160.
1031 96. Bell RE, Ferraccioli F, Creyts TT, Braaten D, Corr H, Das I, Damaske D, Frearson N,
1032 Jordan T, Rose K, Studinger M, Wolovick M. 2011. Widespread Persistent Thickening
1033 of the East Antarctic Ice Sheet by Freezing from the Base. Science 331:1592–1595.

1034 97. Gow AJ, Ueda HT, Garfield DE. 1968. Antarctic Ice Sheet: Preliminary Results of First
1035 Core Hole to Bedrock. Science 161:1011–1013.
1036 98. Christner BC. 2002. Incorporation of DNA and Protein Precursors into
1037 Macromolecules by Bacteria at -15oC. Applied and Environmental Microbiology
1038 68:6435–6438.
1039 99. Amato P, Doyle SM, Battista JR, Christner BC. 2010. Implications of Subzero
1040 Metabolic Activity on Long-Term Microbial Survival in Terrestrial and
1041 Extraterrestrial Permafrost. Astrobiology 10:789–798.
1042 100. Rignot E, Jacobs SS. 2002. Rapid Bottom Melting Widespread near Antarctic Ice
1043 Sheet Grounding Lines. Science 296:2020–2023.
1044 101. Jung J, Yoo K-C, Rosenheim BE, Conway TM, Lee JI, Yoon HI, Hwang CY, Yang K, Subt
1045 C, Kim J. 2019. Microbial Fe(III) reduction as a potential iron source from Holocene
1046 sediments beneath Larsen Ice Shelf. Nat Commun 10:1–10.
1047
1048
1049
1050
1051
1052
1053
1054
1055
1056

1057 **TABLES**

1058 **Table 1.** Description of basal ice types collected in this study

Type	Glacier	Temp (°C)	Description[c]
Clean ice	Taylor	-15[a]	debris-free ice
Banded ice	Taylor	-15[a]	finely stratified layers of debris and ice, layers range in thickness from a few mm to several cm
Solid ice	Taylor	-15[a]	composed primarily of frozen debris with only interstitial ice, no visible layering
Dispersed ice	Matanuska	~0[b]	contains scattered debris aggregated into small clusters, no visible layering

[a]Montross *et al.*, 2014. [b]Lawson *et al.*, 1998. [c]Hubbard *et al.*, 2009

1059

1060 **Table 2.** Cell counts, biomass estimates, and yield of DNA and RNA extracted from basal ice
1061 samples. Sediment-rich basal ice facies are highlighted in gray.
1062

	Cell Density[a]	Yield (pg g^{-1} ice)		Biomass Estimates	
Sample	cells g^{-1} ice	DNA	RNA	genomes[b] g^{-1} ice	ATP (pg g^{-1} ice)
Clean07	0.3 - 0.5 $\times 10^3$	4.7	0.7	1.9 $\times 10^3$	<0.01 - 0.04
Clean09	n.d.	1.4	n.d.	0.6 $\times 10^3$	n.d.
Banded07	1.8 - 18.2 $\times 10^3$	1.7 $\times 10^4$	2.3	6.8 $\times 10^6$	n.d.
Banded09	n.d.	1.6 $\times 10^4$	0.8	6.5 $\times 10^6$	0.24 - 2.8
Solid	6.7 $\times 10^3$	1.4 $\times 10^4$	1.2	5.7 $\times 10^6$	<0.01
Dispersed	n.d.	9.9 $\times 10^4$	3.2	4.0 $\times 10^7$	0.06 - 0.14

[a]Doyle et al. 2013. [b]Number of microbial genomes estimated using 2.5 fg of DNA per genome. n.d.= no data

1063

1064

1065

1066

1067

1068

1069

1070

1071 **FIGURE LEGENDS**

1072 **Figure 1. [A]** Relative abundances of microbial lineages observed in basal ice based on the
1073 use of DNA and RNA templates for detecting 16S rRNA sequences. The graph displays the
1074 highest resolution classification for the most abundant taxa and was constructed as
1075 follows: First, ASVs were clustered by genus and any having a relative abundance ≥20% in
1076 at least one of the samples were plotted. This procedure was subsequently repeated with
1077 the remaining unplotted ASVs at the rank of family, order, class, and finally phylum. Any
1078 remaining rare taxa left after this procedure were not plotted. The bottom plot was scaled
1079 to reduce inflated relative abundance biases introduced during curation. **[B]** Scatter plots
1080 of potentially active ASVs within four types of basal ice. Each point represents an individual
1081 ASV. The dotted-line indicates a 1:1 ratio between the RNA- and DNA-based 16S rRNA
1082 libraries. Gray points denote ASVs observed only in the DNA-based libraries. In the banded
1083 basal ice plot, circles denote ASVs from the Banded07 sample while squares denote ASVs
1084 from the Banded09 sample. Detected ASVs in each plot denotes the number of ASVs
1085 observed in both the RNA- and DNA-based 16S rRNA libraries.

1086

1087 **Figure 2.** Microbial alpha diversity (Shannon) within various perennially frozen
1088 environments.

1089

1090 **Figure 3.** Hierarchical cluster analysis of UF distances between samples using Ward's
1091 minimum variance method. The significance of each node was calculated with a Monte
1092 Carlo simulation using the 'sigclust2' R package. Family-wise error rate (FWER) was

1093 controlled across the dendrogram using a sequential testing procedure starting at the
1094 central node.
1095
1096 **Figure 4. [Left]** RDA triplot of the distribution of 1627 microbial lineages across five
1097 different perennially frozen environments. Colored circles represent individual samples.
1098 Centroids of each environment type are indicated with an "×". Plus signs (+) represent
1099 microbial lineages. The purple circle denotes the equilibrium contribution of the overall
1100 model and delineates lineages which substantially constrained the overall ordination.
1101 Those lineages are highlighted in red. **[Right]** Magnitude of the scalar projections of these
1102 36 lineages onto the centroids for each ice types approximates that lineage's association
1103 with that frozen environment. Scalar projections smaller than the equilibrium contribution
1104 were considered inconclusive and marked gray. Positive and negative associations are
1105 black and red, respectively.
1106
1107 **Figure 5.** Distance-based redundancy analysis of Aitchison distances between different
1108 perennially frozen environments. Colored circles represent centroids of each study's
1109 samples. Black triangles represent individual early studies of basal ice and permafrost
1110 based on Sanger sequencing of 16S rRNA clone libraries.
1111
1112
1113
1114
1115

SUPPLEMENTAL MATERIAL LEGENDS

Figure S1. [A] A subglacial tunnel was excavated into the basal zone of Taylor Glacier's northern lateral margin. **[B]** View from inside one of the excavation tunnels. **[C]** During the 2007 expedition, a vertical shaft was excavated, and a stratigraphic sequence of multiple basal ice types was sampled. **[D]** During the 2009 expedition, a large chamber was excavated to sample a horizon of debris-rich banded basal ice.

Figure S2. An exposed horizon of debris-rich basal ice near the terminus of Matanuska Glacier, Alaska. The sampled area, collected using an electric chainsaw, is highlighted inside the yellow box.

Figure S3. Examples of each type of basal ice analyzed in this study. Clean ice, banded ice, and solid ice were collected from Taylor Glacier, Antarctica. Dispersed ice was collected from Matanuska Glacier, Alaska.

Figure S4. Hierarchical cluster analysis of wUF distances between samples using Ward's minimum variance method. The significance of each node was calculated with a Monte Carlo simulation using the 'sigclust2' R package. Family-wise error rate (FWER) was controlled across the dendrogram using a sequential testing procedure starting at the central node. The three dashed branches in the dendogram were lengthened slightly to improve legibility and are thus not to scale.

1138 **Figure S5.** Heatmap of the 40 taxa identified in five early 16S rRNA clone library studies of
1139 icy environments. Red stars denote 'indicator' microbial taxa which were identified in the
1140 overall meta-analysis (Fig. 4). Taxa abundances were transformed with a Hellinger
1141 transformation to facilitate a clearer visual comparison between abundant and sparse taxa.
1142
1143 **Table S1A.** Amount of basal ice, after decontamination, used for either DNA or RNA
1144 extraction.
1145
1146 **Table S1B.** Description of each sample included in the meta-analysis.
1147
1148 **Table S1C.** DADA2 filtering and curation parameters during meta-analysis.
1149
1150 **Table S1D.** DADA2 pipeline statistics for each sample in the meta-analysis.
1151
1152 **Table S1E.** Shared ASVs between all four basal ice types.
1153
1154 **Table S1F.** Potentially active ASVs within each type of basal ice.

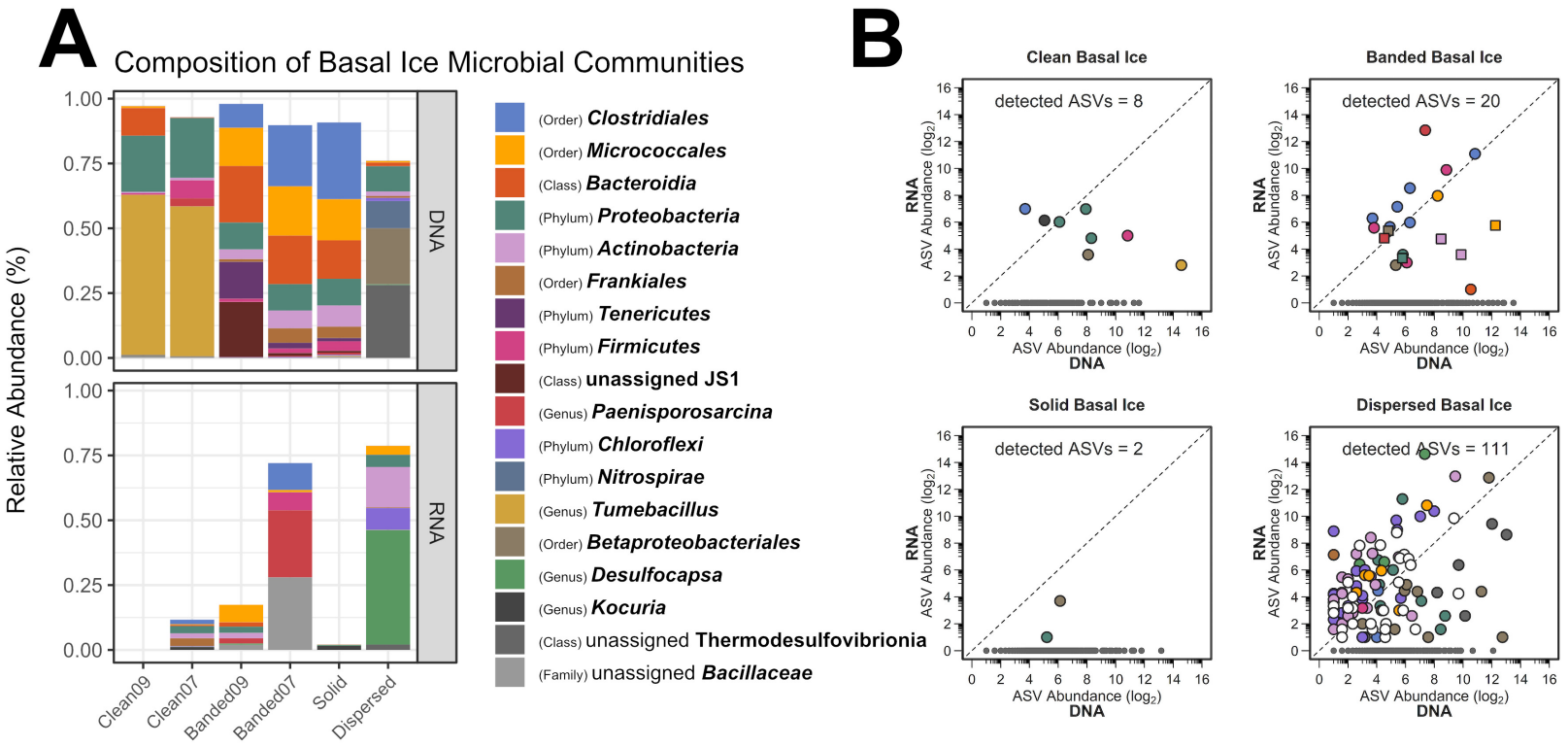
A
Composition of Basal Ice Microbial Communities
Relative Abundance (%)
DNA
RNA
Clean09
Clean07
Banded09
Banded07
Solid
Dispersed
(Order) Clostridiales
(Order) Micrococcales
(Class) Bacteroidia
(Phylum) Proteobacteria
(Phylum) Actinobacteria
(Order) Frankiales
(Phylum) Tenericutes
(Phylum) Firmicutes
(Class) unassigned JS1
(Genus) Paenisporosarcina
(Phylum) Chloroflexi
(Phylum) Nitrospirae
(Genus) Tumebacillus
(Order) Betaproteobacteriales
(Genus) Desulfocapsa
(Genus) Kocuria
(Class) unassigned Thermodesulfovibrionia
(Family) unassigned Bacillaceae
B
Clean Basal Ice
detected ASVs = 8
Banded Basal Ice
detected ASVs = 20
Solid Basal Ice
detected ASVs = 2
Dispersed Basal Ice
detected ASVs = 111
RNA ASV Abundance (log2)
DNA ASV Abundance (log2)

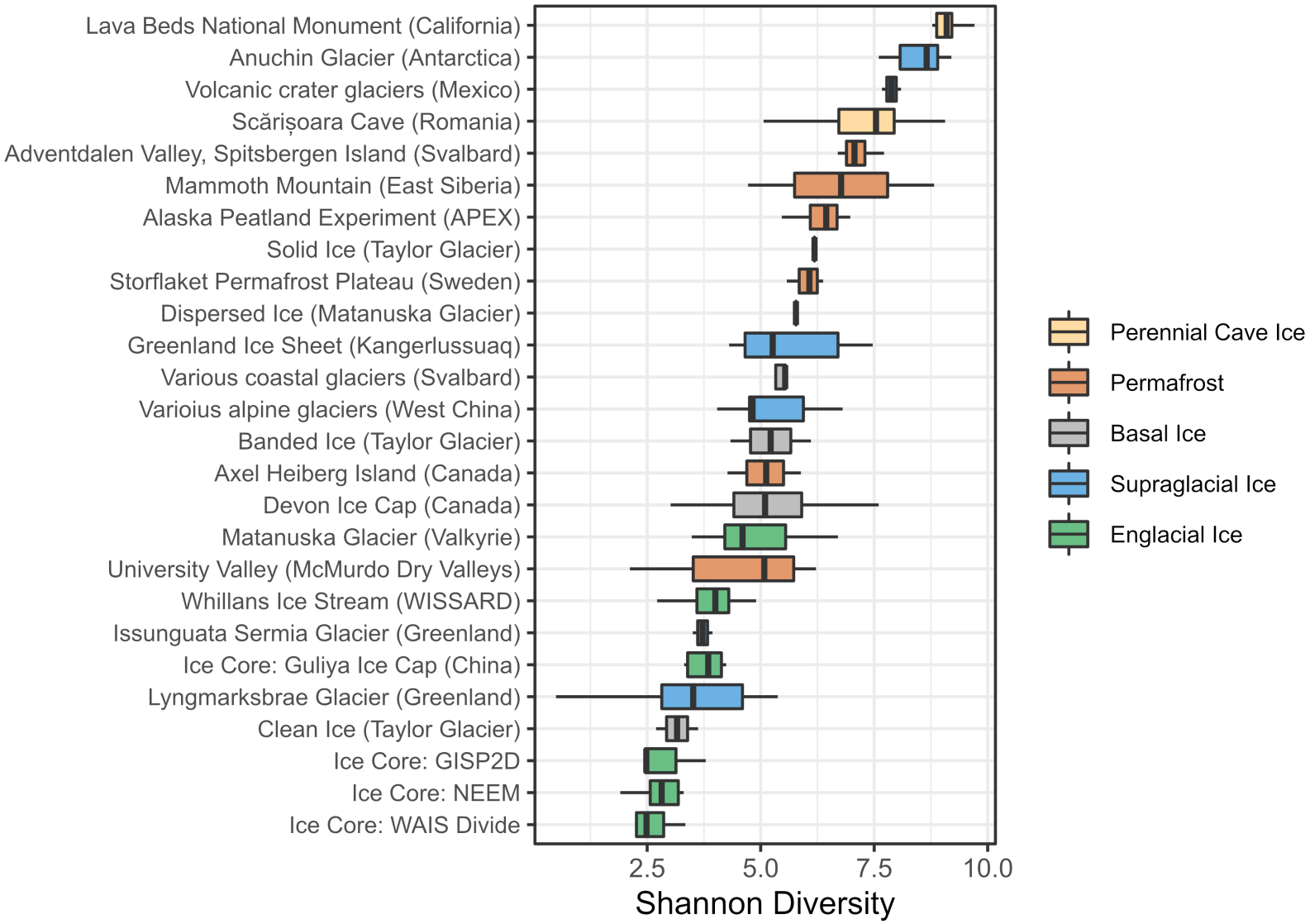
Lava Beds National Monument (California)
Anuchin Glacier (Antarctica)
Volcanic crater glaciers (Mexico)
Scărișoara Cave (Romania)
Adventdalen Valley, Spitsbergen Island (Svalbard)
Mammoth Mountain (East Siberia)
Alaska Peatland Experiment (APEX)
Solid Ice (Taylor Glacier)
Storflaket Permafrost Plateau (Sweden)
Dispersed Ice (Matanuska Glacier)
Greenland Ice Sheet (Kangerlussuaq)
Various coastal glaciers (Svalbard)
Varioius alpine glaciers (West China)
Banded Ice (Taylor Glacier)
Axel Heiberg Island (Canada)
Devon Ice Cap (Canada)
Matanuska Glacier (Valkyrie)
University Valley (McMurdo Dry Valleys)
Whillans Ice Stream (WISSARD)
Issunguata Sermia Glacier (Greenland)
Ice Core: Guliya Ice Cap (China)
Lyngmarksbrae Glacier (Greenland)
Clean Ice (Taylor Glacier)
Ice Core: GISP2D
Ice Core: NEEM
Ice Core: WAIS Divide
2.5
5.0
7.5
10.0
Shannon Diversity
Perennial Cave Ice
Permafrost
Basal Ice
Supraglacial Ice
Englacial Ice

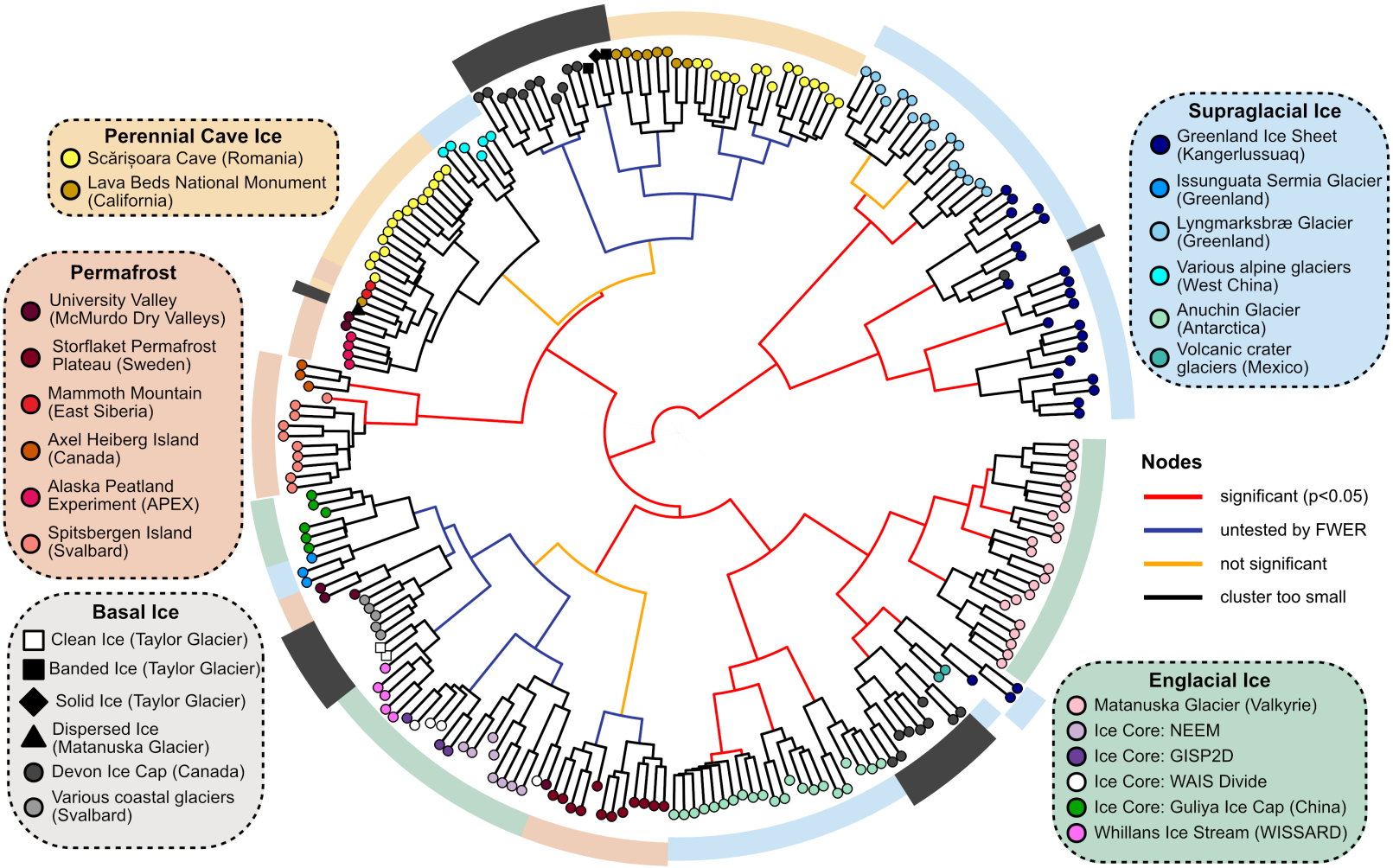
Perennial Cave Ice
Scărișoara Cave (Romania)
Lava Beds National Monument (California)
Permafrost
University Valley (McMurdo Dry Valleys)
Storflaket Permafrost Plateau (Sweden)
Mammoth Mountain (East Siberia)
Axel Heiberg Island (Canada)
Alaska Peatland Experiment (APEX)
Spitsbergen Island (Svalbard)
Basal Ice
Clean Ice (Taylor Glacier)
Banded Ice (Taylor Glacier)
Solid Ice (Taylor Glacier)
Dispersed Ice (Matanuska Glacier)
Devon Ice Cap (Canada)
Various coastal glaciers (Svalbard)
Supraglacial Ice
Greenland Ice Sheet (Kangerlussuaq)
Issunguata Sermia Glacier (Greenland)
Lyngmarksbræ Glacier (Greenland)
Various alpine glaciers (West China)
Anuchin Glacier (Antarctica)
Volcanic crater glaciers (Mexico)
Nodes
significant (p<0.05)
untested by FWER
not significant
cluster too small
Englacial Ice
Matanuska Glacier (Valkyrie)
Ice Core: NEEM
Ice Core: GISP2D
Ice Core: WAIS Divide
Ice Core: Guliya Ice Cap (China)
Whillans Ice Stream (WISSARD)

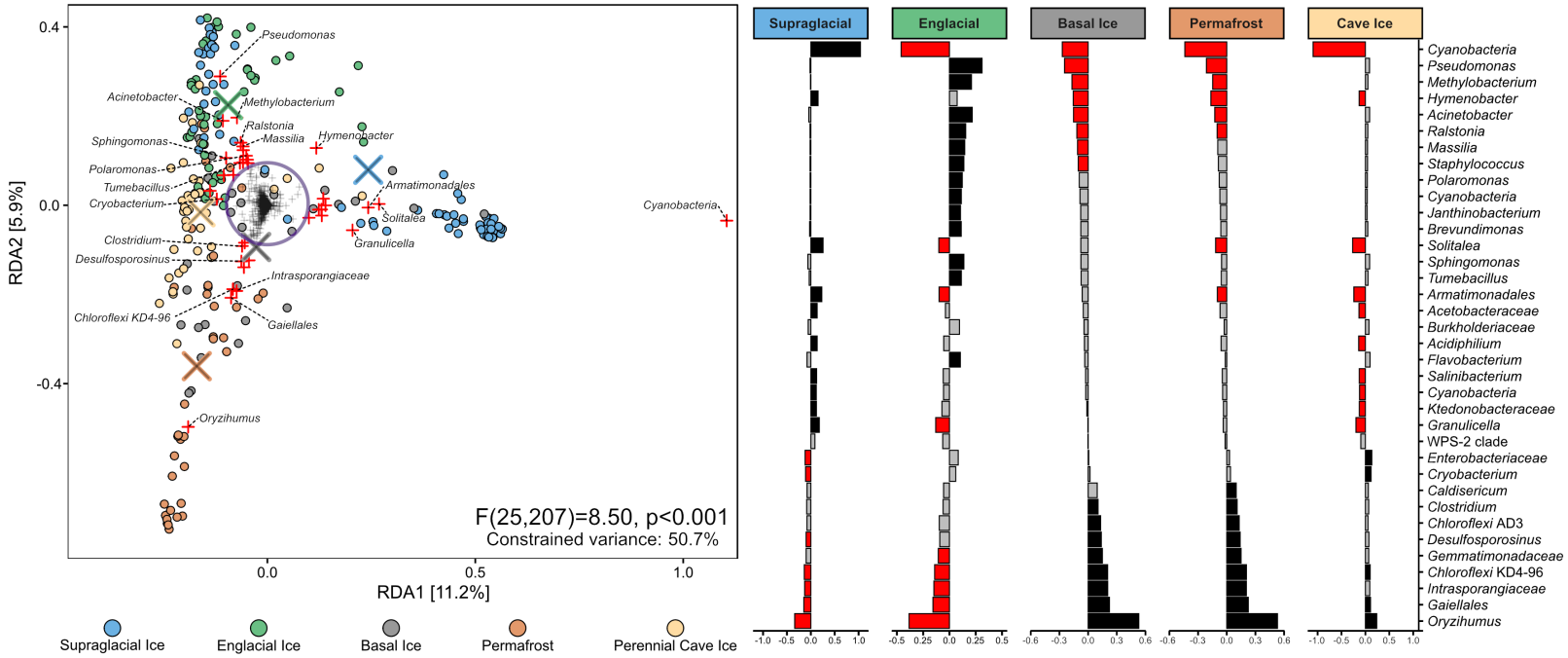
Pseudomonas
Acinetobacter
Methylobacterium
Ralstonia
Massilia
Sphingomonas
Hymenobacter
Polaromonas
Tumebacillus
Cryobacterium
Armatimonadales
Solitalea
Granulicella
Cyanobacteria
Clostridium
Desulfosporosinus
Intrasporangiaceae
Chloroflexi KD4-96
Gaiellales
Oryzihumus
F(25,207)=8.50, p<0.001
Constrained variance: 50.7%
RDA1 [11.2%]
RDA2 [5.9%]
Supraglacial Ice
Englacial Ice
Basal Ice
Permafrost
Perennial Cave Ice
Supraglacial
Englacial
Basal Ice
Permafrost
Cave Ice
Cyanobacteria
Pseudomonas
Methylobacterium
Hymenobacter
Acinetobacter
Ralstonia
Massilia
Staphylococcus
Polaromonas
Cyanobacteria
Janthinobacterium
Brevundimonas
Solitalea
Sphingomonas
Tumebacillus
Armatimonadales
Acetobacteraceae
Burkholderiaceae
Acidiphilium
Flavobacterium
Salinibacterium
Cyanobacteria
Ktedonobacteraceae
Granulicella
WPS-2 clade
Enterobacteriaceae
Cryobacterium
Caldisericum
Clostridium
Chloroflexi AD3
Desulfosporosinus
Gemmatimonadaceae
Chloroflexi KD4-96
Intrasporangiaceae
Gaiellales
Oryzihumus

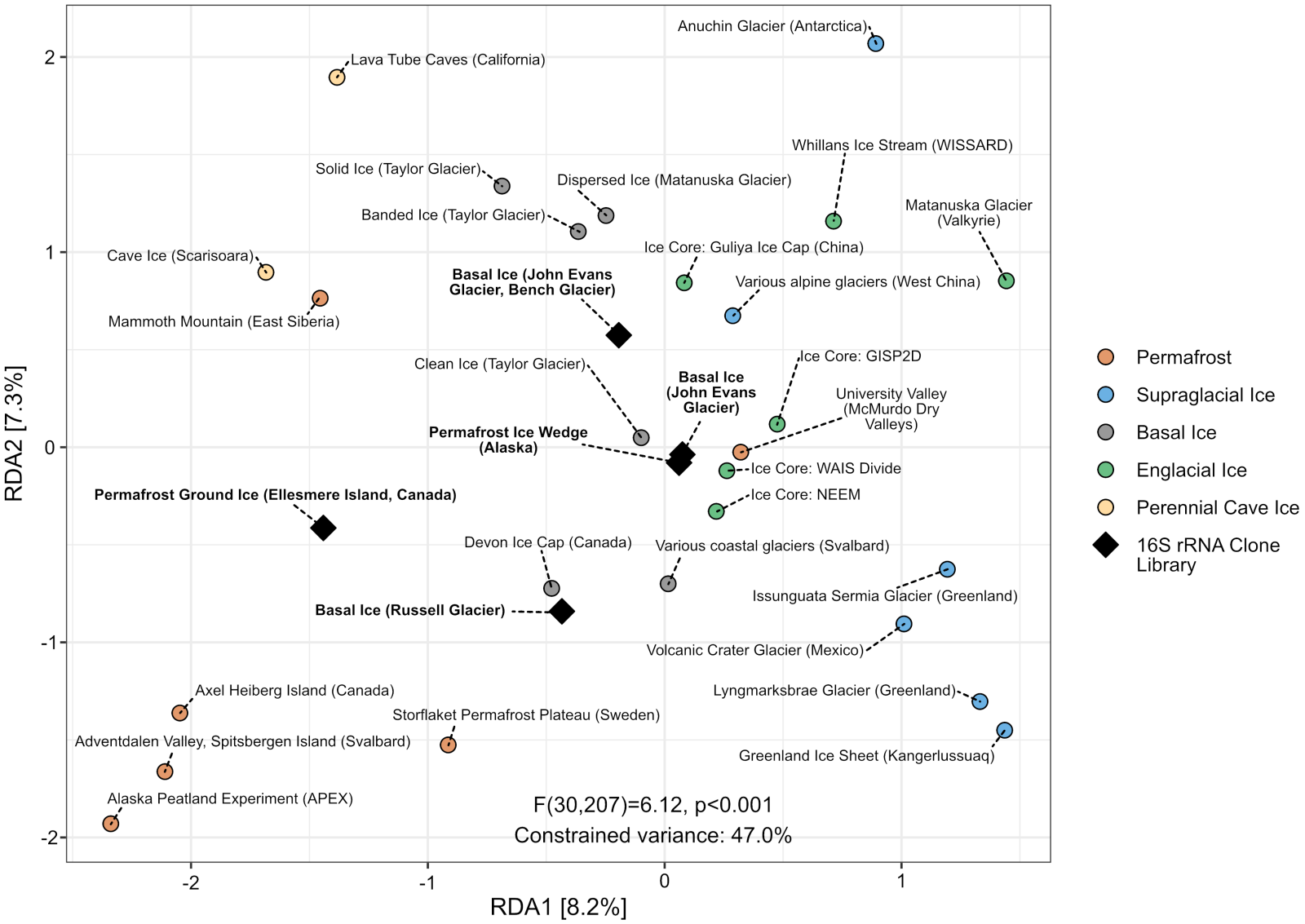
Anuchin Glacier (Antarctica)
Lava Tube Caves (California)
Whillans Ice Stream (WISSARD)
Solid Ice (Taylor Glacier)
Dispersed Ice (Matanuska Glacier)
Banded Ice (Taylor Glacier)
Matanuska Glacier (Valkyrie)
Cave Ice (Scarisoara)
Ice Core: Guliya Ice Cap (China)
Basal Ice (John Evans Glacier, Bench Glacier)
Various alpine glaciers (West China)
Mammoth Mountain (East Siberia)
Ice Core: GISP2D
Clean Ice (Taylor Glacier)
Basal Ice (John Evans Glacier)
University Valley (McMurdo Dry Valleys)
Permafrost Ice Wedge (Alaska)
Ice Core: WAIS Divide
Permafrost Ground Ice (Ellesmere Island, Canada)
Ice Core: NEEM
Devon Ice Cap (Canada)
Various coastal glaciers (Svalbard)
Issunguata Sermia Glacier (Greenland)
Basal Ice (Russell Glacier)
Volcanic Crater Glacier (Mexico)
Axel Heiberg Island (Canada)
Lyngmarksbrae Glacier (Greenland)
Storflaket Permafrost Plateau (Sweden)
Adventdalen Valley, Spitsbergen Island (Svalbard)
Greenland Ice Sheet (Kangerlussuaq)
Alaska Peatland Experiment (APEX)
F(30,207)=6.12, p<0.001
Constrained variance: 47.0%
RDA2 [7.3%]
RDA1 [8.2%]
2
1
0
-1
-2
-2
-1
0
1
Permafrost
Supraglacial Ice
Basal Ice
Englacial Ice
Perennial Cave Ice
16S rRNA Clone Library